

Quantifying the impact of synoptic weather types and patterns on energy fluxes of a marginal snowpack

Andrew Schwartz¹, Hamish McGowan¹, Alison Theobald², Nik Callow³

¹Atmospheric Observations Research Group, University of Queensland, Brisbane, 4072, Australia

²Department of Environment and Science, Queensland Government, Brisbane, 4000, Australia

³School of Agriculture and Environment, University of Western Australia, Perth, 6009, Australia

Correspondence to: Andrew J. Schwartz (Andrew.Schwartz@uq.edu.au)

Abstract.

Synoptic weather patterns are investigated for their impact on energy fluxes driving melt of a marginal snowpack in the Snowy Mountains, southeast Australia. K-means clustering applied to ECMWF ERA-Interim data identified common synoptic types and patterns that were then associated with in-situ snowpack energy flux measurements. The analysis showed that the largest contribution of energy to the snowpack occurred immediately prior to the passage of cold fronts through increased sensible heat flux as a result of warm air advection (WAA) ahead of the front. Shortwave radiation was found to be the dominant control on positive energy fluxes when individual synoptic weather types were examined. As a result, cloud cover related to each synoptic type was shown to be highly influential on the energy fluxes to the snowpack through its reduction of shortwave radiation and reflection/emission of longwave fluxes. As single-site energy balance measurements of the snowpack were used for this study, caution should be exercised before applying the results to the broader Australian Alps region. However, this research is an important step towards understanding changes in surface energy flux as a result of shifts to the global atmospheric circulation as anthropogenic climate change continues to impact marginal winter snowpacks.

1 Introduction

1.1 Synoptic weather influences on snowpack processes

Water generated in mountainous regions is a commodity that over 50% of the world's population depends on for daily life (Beniston, 2003). Arguably, the most important role in the generation and regulation of these water resources is that of montane snowpacks. These have been referred to as "water towers" (Viviroli et al., 2007) due to their capabilities for storage and slow releases of meltwater. Many snowpacks are undergoing reductions in spatial and temporal extent as a result of anthropogenic climate change (Pachauri et al., 2014). Understanding the physical drivers of snowpack ablation, including synoptic-scale influences, is critical to help assess future water resource availability in mountainous regions as climate change continues.

Snowfall has been related to synoptic weather types in numerous studies globally including in Athens (Prezerakos and Angouridakis, 1984), the central and eastern United States (Goree and Younkin, 1966), the Tibetan Plateau (Ueno, 2005), Budapest (Bednorz, 2008a), and the central European lowlands (Bednorz, 2011). However, work on relationships between snowmelt and synoptic weather types is relatively scarce. Bednorz (2008b) identified increased air temperature and rain-on-snow events as causes for rapid snowmelt ($> 5 \text{ cm day}^{-1}$) in the Polish-German lowlands as a result of west-southwest airflows over Central Europe during positive phases of the North Atlantic Oscillation (NAO). Similar work has been conducted in North America by Grundstein and Leathers (1998) who were able to identify three main synoptic weather types responsible for significant snowmelt events

41 on the northern Great Plains, all of which included cyclonic influence with different low pressure centre locations
42 and warm air advection to the region. While some knowledge exists on synoptic drivers of snowpack ablation,
43 further research is needed to understand synoptic effects on ablation processes over snowpacks with varying
44 characteristics.

45 Marginal snowpacks are characterised by high snow density and internal temperatures, making them susceptible
46 to melt from energy input throughout much of the season and particularly sensitive to even subtle shifts in
47 available energy. Anthropogenic climate change has led to changes in snowpack and precipitation properties
48 globally (Adam et al., 2009; Stewart, 2009) and regions that have been historically categorized as having lower
49 temperatures have begun developing marginal characteristics as temperatures increase. However, research related
50 to synoptic influences on the surface energy balance over marginal snowpacks as defined by Bormann et al. (2013)
51 are rare. Hay and Fitzharris (1988) studied the influence of different synoptic weather types on glacier ablation
52 and snowpack melt, while Neale and Fitzharris (1997) used surface energy flux measurements to determine which
53 synoptic types resulted in highest ablation in the Southern Alps, New Zealand. These studies found net radiation
54 was the dominant term in ablation, but also noted that the contributions made by each term varied largely
55 depending on the synoptic type and its meteorology. A common characteristic between these studies and others
56 in various regions is that they focused primarily on the surface meteorology for synoptic classifications rather
57 than multiple level analysis, which enables insight to the potential influence of mid and upper-level atmospheric
58 conditions on surface – atmosphere energy exchanges. Regardless, no analysis at any level exists on synoptic type
59 influence on snowpack ablation within Australia.

60 **1.2 The Australian snowpack**

61 Characteristics of the snowpack in the Australian Alps have been examined in a number of studies with focus on
62 spatial and temporal snow cover variability (Budin, 1985; Duus, 1992), influence on catchment hydrology (Costin
63 and Gay, 1961), the energetics of snowpack melt (Bilish et al., 2018), and isotopic composition of precipitation
64 (Callow et al., 2014). Given observed declines in snow cover, climate change has become a central focus of this
65 research (Chubb et al., 2011; Hennessy et al., 2008; Nicholls, 2005; Reinfelds et al., 2014; Whetton et al., 1996) as
66 any changes to energy flux over the region will significantly impact the already marginal snowpack. Di Luca et
67 al. (2018) showed that snow cover extent in the Australian Alps is expected to undergo reductions of 15% by 2030
68 and 60% by 2070 due to decreases in snowfall quantity and increases in temperature. Observations indicate that
69 reduction in snow cover is already occurring with shortened annual periods of wintertime precipitation. Nicholls
70 (2005) found reductions of 10% and 40% in the maximum snow depth and snow depth at the first October
71 measurement respectively from 1962 to 2002. In addition, wintertime precipitation was shown to have reduced
72 by an average of 43% in high elevation regions from 1990 to 2009 (Chubb et al., 2011), though much of this could
73 have been due to several severe droughts that occurred during the study period. Fiddes et al. (2015a) showed that
74 snowfall, snow accumulation, and snow depth were highly correlated with temperature and that warming, as a
75 result of climate change, could lead to further reductions in the southeast Australia (SEA) snowpack. The
76 importance of the water generated in the Australian Alps, reduction in wintertime precipitation amounts and
77 frequency, and high spatiotemporal variability of snow accumulation and ablation (Budin, 1985) warrants an
78 understanding of the energetics of Australia's snowpack as they pertain to the influences of shifting synoptic-scale
79 circulations.

80 **1.3 Synoptic weather types and trends in the Australian Alps**

81 The Australian Alps is a marginal snowpack environment (Bilish et al., 2019; Bilish et al., 2018), where
82 precipitation is crucial to agriculture, the generation of hydroelectric energy, and recreation. Water generated in
83 the Australian Alps contributes to agriculture in the Murray Darling Basin that accounts for 62% of Australia's
84 water use for irrigation (Australian Bureau of Statistics, 2020). A maximum in precipitation in the Australian Alps
85 typically occurs during the cooler months of June to September when it falls as snow at elevations above 1400 m,
86 and accounts for twice as much precipitation as during the warmer periods of the year (Chubb et al., 2011). While
87 the snowpack typically exists for relatively short periods compared to those of other regions where winter
88 temperatures are lower and higher snowfall amounts occur such as parts of the European Alps and Rocky
89 Mountains, USA, it is still a vital resource for SEA.

90 Synoptic weather types in SEA have been changing in recent decades in response to the impact of climate change
91 on background climate states (Theobald et al., 2016). Pepler et al. (2019) noted anti-cyclone increases of 20-30%
92 in southern Australia and 31-36% in the Tasman Sea during 1960-1979 and 1979-2014 with higher increases
93 during the cool season (May-October). In addition, atmospheric fronts are expected to shift southward (Catto et
94 al., 2014) and predicted global warming driven increases in Southern Annular Mode (SAM) value will result in
95 the poleward shift of general synoptic systems (Cai et al., 2005). This would likely result in significant reductions
96 to snowpack as SAM has been shown to have the highest impact on snow depth and snow season length at
97 Spencers Creek in the Australian Alps with reductions up to 32% during years where the June-September SAM
98 is greater than 0.7 (Pepler et al., 2015).

99 Significant work has been conducted on identification of patterns and trends in Australian synoptic climatology
100 as it pertains to precipitation variability (Theobald et al., 2016; Chubb et al., 2011; Pook et al., 2014; 2010; Pook et
101 al., 2006; 2012; Fiddes et al., 2015b). However, impacts on surface energy fluxes as a result of synoptic types have
102 not been explored as they have in other regions. The objective of this study is to identify the synoptic weather
103 types that contribute the highest amounts of energy to the Pipers Creek catchment headwaters snowpack. This is
104 accomplished through: 1) the identification and classification of common synoptic types during periods of
105 homogeneous snow cover, 2) attribution of snowpack energy flux characteristics to each synoptic type, and 3)
106 construction of energy balance patterns as they pertain to common synoptic patterns/progressions.

107 **2 Methods**

108 **2.1 Study site and climate**

109 Energy flux measurements were made 16 km west of Lake Jindabyne at the Pipers Creek catchment headwaters
110 (36.417°S, 148.422°E) at an elevation of 1828 m in the Snowy Mountains, Kosciuszko National Park, New South
111 Wales (NSW), Australia (Figure 1). The surrounding areas contain a mixture of living and dead *Eucalyptus*
112 *pauciflora* (Snow Gum) trees and open grassland areas with fens and alpine bogs. Many of the Snow Gums were
113 impacted by fire in 2003, and have experienced slow regrowth. The site chosen at the Pipers Creek catchment
114 headwaters contains alpine bog and Eucalypt woodland that are “the two most common types in the broader
115 region, together representing 47% of the total area above 1400-m elevation” (Bilish et al., 2018, p. 3839). Gellie
116 (2005) showed that the *E. pauciflora* woodland was present in five of the fifteen dominant vegetation formations
117 that covers 57% of area within the broader region, while Alpine grassland/bog (including herb fields) accounts
118 for another 8%. The area's mixed characteristics of forested and open grasslands with alpine wetlands within the

119 Pipers Creek study catchment and immediately surrounding the flux tower site used in this study are representative
120 of those found throughout the Australian Alps.

121 The Snowy Mountains are characterized by relatively mild weather conditions compared to other mountain
122 ranges. Winter temperatures are typically around 0°C with mean low temperatures during July (the coldest month)
123 at -5°C and mean high temperatures between 2 to 4°C (Bureau of Meteorology, 2018b) that readily allow for melt
124 of the snowpack. As such, snowpack properties in the catchment are consistent with those of maritime snowpacks
125 that are associated with basal melting, high temperatures, and high wind speeds (Sturm et al., 1995; Bilish et al.,
126 2018).

127 The nature of single-site energy balance studies in complex terrain means that measurements may not be truly
128 representative of the larger area. Terrain-induced flows and aspect/slope at the measurement site can alter radiative
129 exchange and turbulent fluxes resulting in different energy balances over short distances. Therefore, we suggest
130 caution when applying the Pipers Creek catchment headwaters energy balance to the wider area of the Australian
131 Alps. While this is a drawback to single-site studies, this paper aims to take the first step towards broad-scale
132 understanding of synoptic weather on the Snowy Mountains snowpack.

133 **2.2 Instrumentation**

134 The Pipers Creek site (Figure 2) was established on 10 June 2016 and collected data for the 2016 and 2017 winter
135 seasons. The site consisted of a Campbell Scientific eddy covariance (EC) system to measure fluxes of latent (Q_e)
136 and sensible (Q_h) heat at 10 Hz at a height of 3.0 m above ground level (AGL). A Kipp and Zonen CNR4
137 radiometer (3.0 m AGL) was used to measure incoming and outgoing shortwave (K) and longwave (L) radiation
138 to allow for comparisons of all radiation components rather than simply net all-wave radiation (Q^*). Ambient air
139 temperature and relative humidity were measured at the top of the mast by a Vaisala HMP155 probe at ~3.1 m
140 above ground level. A Hukseflux heat flux plate measured ground heat flux (Q_g) at a depth of 5 cm and was placed
141 approximately 0.5 m from the centre of the mast to minimize any influence the mast could have on snow
142 accumulation above the sensor. Surface temperatures were monitored using an Apogee Instruments SI-111
143 infrared radiometer at approximately 2 m from the centre of the mast. Details on the instruments used for each
144 measurement are shown in Table 1.

145 Precipitation data from an ETI Instrument Systems NOAH II weighing gauge located approximately 1 km to the
146 northwest of the energy balance site at elevation of 1761 m was supplied by Snowy Hydro Limited (SHL). A 6 m
147 diameter DFIR shield was used around the gauge in order to prevent wind-related under-catch of snowfall
148 (Rasmussen et al., 2012), and was additionally sheltered by vegetation to the west.

149 **2.3 Identification of snow cover periods**

150 Homogeneous snow cover is crucial to accurate measurement and analysis of snowpack energy balance (Reba et
151 al., 2009). Snow cover was considered to be homogeneous when no grass or bush was protruding from the snow
152 surface with the exception of distant patches of *E. pauciflora* trees. Periods with homogeneous snow cover were
153 determined using data from the Pipers Creek instrumentation site and were cross referenced to manual snow
154 measurements made at the Spencers Creek Snow Course 6.6 km northwest of the Pipers Creek field site (Snowy
155 Hydro Ltd, 2018). Periods with surface temperatures above 1.5°C as measured by the SI-111 infrared radiometer

156 that did not correspond to rain-on-snow events and periods with albedo measurements less than 0.40 (Robock,
157 1980) were considered to have heterogeneous snow cover and were eliminated.

158 **2.4 Synoptic classification of snow cover days**

159 Synoptic weather type classification of homogeneous snow cover days was conducted using synoptic typing
160 methods adapted from Theobald et al. (2015). European Centre for Medium-Range Weather Forecasts (ECMWF)
161 ERA-Interim reanalysis data (Dee et al., 2011) with a $0.75^\circ \times 0.75^\circ$ resolution was obtained for each day from 10
162 June 2016 through 31 October 2017. This date range was chosen to ensure inclusion of all potential dates with
163 snow cover during the 2016 and 2017 snow seasons after the initial instrument tower installation on 10 June 2016.
164 Variables included in the reanalysis data consisted of mean daily values of Mean Sea Level Pressure (MSLP);
165 temperature and relative humidity at 850, 700, 500, and 250 hPa; wind vectors at 10 m AGL, 850, 700, 500, and
166 250 hPa; and 1000-500 hPa geopotential heights. The domain of the included variables was limited to $20^\circ\text{S} - 46^\circ\text{S}$
167 and $120^\circ\text{E} - 160^\circ\text{E}$, ensuring coverage of synoptic scale systems affecting the Australian Alps.

168 Focus was placed on analysis of temperature (T_d) and relative humidity (RH) values because of their impact on
169 Q_e , Q_h , and radiative fluxes (Reba et al., 2009; Ruckstuhl et al., 2007; Allan et al., 1999; Webb et al., 1993). Relative
170 humidity values at 850, 700, and 500 hPa were used to investigate the potential influence of cloud cover. MSLP
171 and wind vector analysis at the 850, 700, 500, and 250 hPa levels allowed for the identification of T_d and RH
172 advection (Pook et al., 2006) into the Australian Alps. Thickness between 1000-500 hPa was used to determine
173 frontal positions relative to the Australian Alps (Pook et al., 2006) and accordingly the Pipers Creek field site.

174 The method used for synoptic comparison of energy flux characteristics was adopted from the approach of similar
175 types of studies that used “days” as the temporal period for analysis in the Snowy Mountains region (Theobald et
176 al., 2016; Theobald et al., 2015; Chubb et al., 2011; Fiddes et al., 2015b) and glacier/snowpack energy balance (Hay
177 and Fitzharris, 1988; Neale and Fitzharris, 1997). “Days”, periods lasting twenty-four hours from 00Z to 23:59Z,
178 were considered optimal to determine radiative flux characteristics (diurnal radiation cycle) that may be missed
179 on smaller time scales. While the use of UTC days meant that the synoptic characteristics corresponded to local
180 days by an offset by 10 hours (00:00 UTC = 10:00 AEST), the effects of the synoptic conditions on terrain-induced
181 flows would be the same regardless of whether they aligned with the local day. Overall, the use of UTC days
182 allowed for determination of short-term energy fluxes that can also be easily compared over several months, thus
183 being most appropriate for the entire snow season. Examination of higher temporal resolution snowpack energy
184 balance at a collocated site can be found in Bilish et al. (2018).

185 Days within the ERA-Interim data that matched snow cover days were extracted and analysed using the k-means
186 clustering algorithm developed by Theobald et al. (2015). The algorithm was tested for 1-20 clusters and an elbow
187 plot of the cluster distances was used to identify the optimum number of clusters (Theobald et al., 2015), which
188 was seven. The identification of an elbow in the plot at seven clusters indicates a reduction to the benefit of adding
189 additional clusters as the sum of distances for additional clusters fails to yield significant reductions beyond that
190 point (Wilks, 2011).

191 Clustering of the synoptic conditions for each day was verified through manual analysis of MSLP and 500 hPa
192 charts from the Australian Bureau of Meteorology (BOM) (Bureau of Meteorology, 2018a). Cloud cover for each
193 type was investigated and verified through the use of visible and infrared band Himawari-8 satellite data

194 (<https://www.ncdc.noaa.gov/gibbs/>) at three hour increments from 00Z to 21Z, (10:00 AEST to 07:00 AEST) with
195 one of three categories assigned to each day studied; 1) no cloud cover, 2) partial cloud cover, or 3) complete
196 cloud cover. Cloud cover was investigated throughout the days to ensure that all effects of cloud cover on energy
197 balance were represented.

198 Manual verification of the k-means clustering algorithm using BOM synoptic charts identified four days (2.45%)
199 out of the 163 classified during the 2016 and 2017 seasons that had been classified incorrectly and they were
200 subsequently moved to their correct synoptic type. Three of the four misclassified days were early (7 June 2016)
201 or late (19 and 22 September 2016) in the snowpack seasons with the fourth occurring in the middle of winter on
202 31 July 2017. Synoptic characteristics from these days tended to be complicated with no discernible dominant
203 features that matched those of classified types. This is likely due to shifting synoptic conditions between seasons
204 related to poleward or equatorial shifts in westerly winds.

205 **2.5 Snowpack energy accounting**

206 Accurate measurement of snowpack energy balance and associated melt can be difficult due to snowpack
207 heterogeneity (Reba et al., 2009) and problems with energy balance closure (Helgason and Pomeroy, 2012). The
208 basic snowpack energy balance can be expressed as:

$$209 \quad Q_m = Q^* + Q_h + Q_e + Q_g + Q_r \quad (1)$$

210 where the energy available for snow melt (Q_m) is equal to the sum of Q^* , Q_h and Q_e , Q_g , and the energy flux to
211 the snowpack from liquid precipitation (Q_r) (Male and Granger, 1981; McKay and Thurtell, 1978). It's important
212 to note that all terms used in the calculation of the snowpack energy balance are net terms (Marks and Dozier,
213 1992; Stoy et al., 2018; Welch et al., 2016). Using net terms allows for conservation of energy within the (ideally)
214 closed energy balance system of the snowpack and aids in more accurately determining contributions of each term
215 to the energy balance.

216 Internal energy storage and melt processes can make calculation of the snowpack energy balance particularly
217 difficult when internal measurements of the snowpack are not available due to problems closing the energy
218 balance (Helgason and Pomeroy, 2012). This is particularly difficult over Australia's snowpack due to its marginal
219 characteristics that result in nearly constant internal snowpack melt. Therefore, Q_m can be more accurately
220 expressed as a residual energy term (Q_{res}) that is defined as the sum of the measured terms in Eq. (1) plus any
221 error in energy balance closure (Q_{ec}):

$$222 \quad Q_{res} = Q^* + Q_h + Q_e + Q_g + Q_r + Q_{ec} \quad (2)$$

223 While Q^* can be used for basic analysis of the snowpack energy balance, a decomposition into its individual
224 components is necessary to understand the role of short and longwave radiation exchange in snowpack energetics
225 (Bilish et al., 2018). Therefore, net radiation should be broken into its net flux terms:

$$226 \quad Q^* = K^* + L^* \quad (3)$$

227 that quantify the net shortwave (K^*) and net longwave (L^*) components.

228 The approach taken within this paper is to examine net radiative flux components individually, similar to the
229 methods used by Bilish et al. (2018), to be precise in the identification of synoptic-scale effects on snowpack
230 energy fluxes through differences in temperature, relative humidity, cloud cover. Q_{res} calculation and
231 comparisons of snowpack energy flux terms were performed using the terms in Eq. (2), but with the net radiation
232 terms (K^* and L^*) used rather than summed as Q^* only. This research uses the energy flux convention where
233 positive values are flux to the snowpack and negative values are flux away from the snowpack.

234 **2.6 Energy flux measurements of synoptic types**

235 Coordinate rotation for EC systems is typically used to account for errors introduced into flux data due to
236 imprecise instrumentation levelling. However, complex terrain can complicate EC measurements through local
237 scale processes such as thermally induced anabatic and katabatic flows, modification and generation of complex
238 terrain-induced flows, and inhomogeneity of terrain. In these areas, coordinate rotation is used to align the eddy
239 covariance coordinate system with the sloping surface and to identify and remove larger scale motions that may
240 be measured with the microscale flows. The Pipers Creek catchment site is located on predominantly level terrain,
241 however, double coordinate rotation was used to process the EC data to ensure terrain-induced influences on
242 airflow were removed (Stiperski and Rotach, 2016).

243 Frequency corrections were made to the EC data to account for sensor response delay, volume averaging, and the
244 separation distance of the sonic anemometer and gas analyser when calculating fluxes. Finally, WPL air density
245 corrections (Webb et al., 1980) were made to account for vertical velocities that exist as a result of changing air
246 mass density through fluxes of heat and water vapour. Quality flags were calculated for Q_h and Q_e using the
247 methods of Mauder and Foken (2011) that assigned a number from 0-2 based on the quality of the fluxes. High
248 quality data that is able to be used for fundamental research was assigned a 0, fluxes assigned a 1 are less accurate
249 but can still be used for long term observations, and fluxes assigned a 2 needed to be removed and gap-filled.

250 Q_h and Q_e flux were calculated using the EC equations:

$$251 \quad Q_h = -\rho C_p (\overline{w'\theta'}) \quad (4)$$

$$252 \quad Q_e = -\rho L_v (\overline{w'q'}) \quad (5)$$

253 where ρ is air density (kg m^{-3}), C_p is the specific heat of air ($1005 \text{ J kg}^{-1} \text{ deg}^{-1}$), $\overline{w'\theta'}$ is the average covariance
254 between the vertical wind velocity w (ms^{-1}) and potential temperature θ (K), L_v is the latent heat of sublimation
255 or vaporization of water (J kg^{-1}), and $\overline{w'q'}$ is the average covariance between the vertical wind velocity w (ms^{-1})
256 and specific humidity q (kg kg^{-1}) (Reba et al., 2009).

257 The calculation of Q_r followed Bilish et al. (2018) and was determined using three separate calculations to
258 establish approximate wet bulb temperature (T_w) (Stull, 2011), the fraction of precipitation falling as rain ($1 -$
259 P_{snow}) (Michelson, 2004), and total rain heat flux (Q_r) based on precipitation accumulation over a 30-minute
260 period.

261 **2.7 Energy flux data quality control and gap-filling**

262 In addition to removing EC measurements assigned a quality flag of 2, Q_e and Q_h values were also removed
263 when water vapour signal strength, a unit-less number calculated from the fraction of beam received compared to

264 that emitted, from the gas analyser was < 0.70 in order to remove erroneous readings during periods of
265 precipitation (Campbell Scientific, 2018; Gray et al., 2018). A seven point moving-median filter was implemented
266 over three iterations to de-spike the data and remove values more than 3.0 standard deviations away from the
267 median values.

268 Pre-existing gaps and gaps introduced into the data by the quality control procedures were filled using linear
269 interpolation described by (Falge et al., 2001a;2001b) and the Random Forest regression technique (Breiman,
270 2001). Linear interpolation of missing Q_e and Q_h values was used for gaps up to 90 minutes in length.
271 Traditionally, mean diurnal variation values are also used for gap filling procedures (Falge et al.,
272 2001a;2001b;Bilish et al., 2018). However, it was determined that using mean values would likely obscure any
273 unique energy balance characteristics of the synoptic types being investigated and, therefore, was not included as
274 a gap-fill strategy for the data.

275 The R programming package randomForest (Liaw and Wiener, 2002) was used to fill gaps in Q_e and Q_h longer
276 than 90 minutes in length. The random forest regression trained to determine Q_e and Q_h flux values was developed
277 using twenty-six atmospheric and soil variables collected in addition to EC measurements. Mean squared errors
278 (MSE)'s were examined for forests with 1-500 trees and it was determined that 150 trees were sufficient to build
279 an accurate model for both Q_e and Q_h . Tests were then conducted to determine the optimal number of variables
280 to be randomly selected at each node that showed 13 variables was optimal for determination of Q_h and 14
281 variables should be used for Q_e . The Q_e and Q_h random forest regression models were tested for their ability to
282 predict values that had been used to train the models by comparing the measured Q_e and Q_h values with the
283 predicted values. Root Mean Squared Error (RMSE) and the Coefficient of Determination (R^2) were determined
284 for each advective flux. Predicted values showed high correlation to measured values with both variables showing
285 R^2 values higher than 0.97. The Q_e regression had a RMSE of 2.56 Wm^{-2} and had lower uncertainty than the Q_h
286 regression that had a RMSE of 4.67 Wm^{-2} .

287 Following quality control procedures, 2571 of the initial 7756 records (33%) remained in the Q_e data and 4019
288 records (52%) remained in the Q_h data. Linear interpolation yielded an addition of 910 Q_e values (12%) and 928
289 Q_h values (12%). The Random Forest regression models were the largest source of gap-filled data with the
290 contribution of an additional 4275 Q_e values (55%) and 2809 Q_h values (36%).

291 **3 Results**

292 Identification of homogeneous snow cover days for the 2016 and 2017 snow seasons (June to October) resulted
293 in 163 total days with 90 days occurring in the 2016 and 73 days in 2017. July, August, and September had the
294 highest number of classifiable days during the period. June and October still had periods with homogenous snow
295 cover, but they became intermittent and fewer classifiable days were in each of the months. This led to fewer
296 periods of study at the beginning and end of the snow seasons when the snowpack was variable, with more in the
297 late winter and early spring months when snow cover was more consistent. Mean surface and cloud characteristics
298 and median daily energy flux characteristics of synoptic types identified during the two seasons are presented in
299 Table 2.

300 **3.1 Synoptic types**

301 **3.1.1 Surface characteristics**

302 The dominance of the subtropical ridge in Australia's mid-latitudes is evident in the synoptic types. Four of the
303 types (T1, T2, T5 and T7) display dominant surface high pressure systems, each with slightly different orientation
304 and pressure centre locations (Figure 3a) resulting in different energy flux characteristics. Dominant south-
305 southwesterly winds from T1 are the result of the high pressure centre being located to the northwest of the study
306 area. T2 has a predominantly zonal flow resulting from an elongated high to the north-northeast. T5 and T7 are
307 characterized by north-northwesterly flow from high pressure centres over the New South Wales
308 (NSW)/Queensland (QLD) coast and directly over the Snowy Mountains region, respectively.

309 T3 is characterized as having dominant northwest winds along a trough axis that is positioned over SEA with a
310 secondary coastal trough extending from southern NSW to the NSW/QLD border. T4 shows a transition from a
311 surface trough that has moved to the east of the study region to a high pressure system that is moving into the area
312 with winds from both features that converge over the Snowy Mountains region. The only synoptic type to have
313 dominant influence from a surface low was T6 that had weak south-southwesterly flow over the region from a
314 weak cut-off low to the east. For the purposes of this research, the identification of cut-off lows follows the
315 characteristics outlined by Chubb et al. (2011) that omits the presence of a closed circulation, but includes a cold
316 anomaly aloft that was cut off from the westerly wind belt.

317 Though characterization of synoptic types is purely statistical, T1, T4, T5, and T6 are considered to be 'transition
318 types' as they have surface pressure characteristics that indicate a change in pressure regime (low – high or high
319 – low) in the upcoming days. T1, T4, and T6 are post-frontal transition types that show high pressure ridging into
320 the region following the passage of a trough that has either moved to the east (T1 and T4) or developed into a
321 weak lee-side cut-off low (T6). T5 shows the approach of a trough from the west and an associated transition to
322 a low pressure system. T2 and T7 show the area under the influence of zonal flow as a result of high pressure
323 systems centred over the area, while T3 shows SEA under the influence of a trough at the time of observations.

324 **3.1.2 Relative humidity and cloud cover**

325 Understanding RH values associated with different synoptic types provides the ability to track types that are
326 favourable for high Q_e exchange with the snowpack. In addition, RH values at all tropospheric levels can have
327 impacts on snowpack energy flux through influences on K^* and L^* exchange via changes to insolation and the
328 absorption and emission of L . The identification of RH characteristics and associated cloud cover is necessary to
329 fully develop energy flux characteristics for each type.

330 Many of the synoptic types display local RH maxima in the Snowy Mountains region at 850 hPa (Figure 3b) and,
331 while T5 has the lowest RH values of all types, it still has slightly higher RH values over the area. The elevation
332 in RH values in the region is most likely caused by changes of air mass thermodynamic properties due to
333 orographic forcing of the mountains (Ahrens, 2012). T4 and T6 had the highest RH values over the region at 850
334 hPa with both being widespread and higher than 90%. T6 shows strong southerly advection of elevated RH values
335 from the tropics along the NSW and QLD coast ahead of troughs at 700 and 500 hPa that are associated with the
336 surface cut-off low.

337 Identification of cloud cover, conducted following the procedures outlined in section 2.4, agreed with the mean
338 RH characteristics of T4 and T6 with both types having 100% cloud cover between partial and complete cloud
339 cover days (Table 2). However, T1, T3, and T5 also had 100% cloud cover occurrence and two of the three (T1
340 and T3) had RH values above 80%. T5 was the only synoptic type with 100% cloud cover and RH value below
341 80%. T6 showed the highest RH values of any type with values greater than 90% over the region at the 700 and
342 500 hPa levels. While not definitive, this would suggest that T6 has deeper or more cloud layers than T4, which
343 likely only has clouds at lower altitudes. T2 and T7 had the lowest percentage of days with any cloud cover, which
344 is confirmed by their low RH values at 700 hPa (<20% & <30%) and 500 hPa (<30% & <40%), respectively. In
345 addition, they were the only two types with cloud-free days with T2 clear sky 25% of the time and T7 having 16%
346 of its days without cloud.

347 **3.1.3 Temperature**

348 Temperature characteristics of synoptic types at low and mid-levels in the atmosphere are crucial to identify those
349 with the highest surface sensible heat flux characteristics. The highest mean temperatures and strongest warm air
350 advection (WAA) in the Snowy Mountains region at 850 hPa (Figure 3c) was found to be from T5 that is driven
351 by converging winds on the back of a high pressure circulation to the east and the leading edge of a trough to the
352 west. T2 and T3 have the second and third highest temperatures, respectively, but have different advection
353 characteristics. T2 shows relatively weak WAA into the Snowy Mountains region associated with zonal flows at
354 850 hPa resulting from the high pressure circulations located to the north (similar to T7). However, T3 shows cold
355 air advection (CAA) associated with dominant winds from the west-northwest.

356 Overall, CAA at 850 hPa can be identified in four of the seven types (T1, T3, T4, and T6) and warm air advection
357 exists in the other three synoptic types (T2, T5, and T7). Of the four CAA types, T1 and T4 advection is being
358 generated through south-southwest and west-southwest winds, respectively, related to high pressure centres to the
359 northwest. Despite a stronger southerly component of dominant CAA winds in T1, temperatures are lower in T4
360 which has a higher westerly component to the wind. T6 shows CAA related to converging winds on the back of a
361 trough to the east and a high to the northwest.

362 **3.1.4 Frequency and duration**

363 The frequency of each synoptic type during the 2016 and 2017 snowpack seasons is shown in Table 2. T3 and T7
364 occurred most frequently with 26.99% (44 days) and 19.02% (31 days) respectively. The higher number of days
365 in T3 and T7 is reflected in the mean type duration that shows these types with the longest duration. This is likely
366 due to these synoptic types occurring in a slower progressing synoptic pattern over multiple days as seen in the
367 mean type duration data (Table 2).

368 Identification of common synoptic circulations, that are comprised of a progression of several synoptic types, and
369 their impact on surface energy balance can aid in the understanding and forecasting of snowpack ablation based
370 on synoptic conditions. In order to identify common synoptic circulations, analysis on common transitions
371 between synoptic types was conducted. Transition probabilities for the 2016 and 2017 seasons were developed
372 similar to those used by Kidson (2000) that detail the likelihood of a synoptic type occurring on the following day
373 given an initial type. The highest transition probabilities were identified for each type and a flowchart was
374 developed based on the most likely synoptic type progressions (Figure 4a). If the highest transition probabilities

375 were within < 0.05 of each other, two paths were plotted. The flowchart shows what would be expected for a basic
376 synoptic-scale circulation at mid-latitudes; a trough propagating eastward into the Snowy Mountains region in T7,
377 T5, and T3; either continued eastward movement of the surface trough (T4) or the development of a weak cut-off
378 low (T6); then transitioning to dominant high pressure over the region again (T2, T1, or T7).

379 **3.2 Energy flux characteristics of synoptic types**

380 It is important to consider the effects of synoptic type frequency when determining primary sources of energy
381 fluxes over long periods, as synoptic types that contribute the most to snowpack ablation may simply have a higher
382 rate of occurrence and lower daily energy flux values than other types. In order to obtain a more detailed
383 understanding of each type's energy flux, median daily energy flux calculated for each type was determined to be
384 a better method of comparison. Therefore, both median daily and total snowpack fluxes over the two seasons
385 (Figures 5 & 6) are presented in MJ m^{-2} to show synoptic type energy flux contributions made at short and longer
386 temporal scales. While initial measurements were made in Wm^{-2} , the use of MJ m^{-2} in this paper allows for easier
387 comparison to other energy balance works conducted on this region (Bilish et al., 2018) as well as research on
388 synoptic weather and energy fluxes in other locations (Welch et al., 2016; Burles and Boon, 2011; Ellis et al.,
389 2011; Hay and Fitzharris, 1988; McGregor and Gellatly, 1996; Granger and Gray, 1990; Neale and Fitzharris, 1997).

390 **3.2.1 Latent and sensible heat flux**

391 Daily Q_e was negative for each of the seven synoptic types (Figure 5a) and the magnitude of the values was shown
392 to correspond to the mean 850 hPa RH values for each type reflecting the site elevation of 1828 m asl. Two of the
393 three types with the lowest RH values (T2 and T5) showed the greatest negative Q_e values and those with the
394 higher RH values (T1 and T6) showed the least amount of Q_e , which is consistent with conditions needed for
395 evaporation from the snowpack. T5 had the second largest negative Q_e values of any type with a median value
396 of $-1.00 \text{ MJ m}^{-2} \text{ day}^{-1}$ which corresponds to its low 850 hPa RH values, the highest observed surface mean daily
397 ambient temperature of $3.5 \text{ }^\circ\text{C}$, and the second lowest observed surface mean RH value of 65% with only T2 being
398 lower (60%). T3 showed the largest release of Q_e from the snowpack with a median value of $-1.11 \text{ MJ m}^{-2} \text{ day}^{-1}$.

399 Overall, negative Q_e was offset by positive Q_h for most synoptic types with the exception of T3 that had mean
400 surface temperatures below zero (-0.83°C) and a measured surface RH value below 90% resulting in more Q_e
401 loss than Q_h gain by the snowpack. Similar to trends seen in Q_e , the highest daily median Q_h values (Figure 5b)
402 were associated with synoptic types with the highest temperatures at 850 hPa (T5, T7, & T2), which coincided
403 with observed temperatures from the energy flux tower (3.48°C , 1.46°C , & 1.89°C). T5 showed the highest daily
404 Q_h values as a result of having the highest temperatures and also has the second lowest Q_e value that is associated
405 with having the lowest RH of any type (60%). Ultimately, when both turbulent terms are considered, T5 had the
406 highest amount of energy flux into the snowpack ($1.49 \text{ MJ m}^{-2} \text{ day}^{-1}$) followed by T7 ($1.40 \text{ MJ m}^{-2} \text{ day}^{-1}$) and T1
407 ($1.00 \text{ MJ m}^{-2} \text{ day}^{-1}$).

408 **3.2.2 Radiation flux**

409 The largest contribution of radiative energy to the snowpack from all synoptic types was K^* which accounted for
410 53-97% of total positive flux (Figure 5c). By comparison, L^* accounted for 61-95% of negative energy flux from
411 the snowpack (Figure 5d) with the highest amounts of loss belonging to the types with the lowest percentage of
412 cloud cover (T1, T2, and T7). Total radiation flux varied largely by synoptic type and was found to be positive in

413 types T3 and T6 and negative for the rest of the types. The two types with positive net radiation had the highest
414 incoming longwave radiation flux values mostly balancing outgoing longwave values. This meant that incoming
415 shortwave radiation was able to dominate Q^* for these types, which resulted in the positive values. The largest
416 loss in Q^* was exhibited by T1, that was 31% higher than the next closest type (T4). The types with net radiation
417 loss (T1, T2, T4, T5, and T7) had values that ranged from $-0.67 \text{ MJ m}^{-2} \text{ day}^{-1}$ (T5) to $-2.78 \text{ MJ m}^{-2} \text{ day}^{-1}$ (T1).
418 However, T4 had dissimilar cloud and RH characteristics to T2 and T7, which had the two lowest cloud cover
419 percentages and two of the lowest RH values. T4 had 100% cloud cover and had an associated reduction in
420 incoming shortwave radiation that allowed the outgoing longwave radiation term to become more dominant than
421 in T2 or T7 and, therefore, gave it the highest Q^* loss of the three.

422 3.2.3 Ground and precipitation heat flux

423 Energy flux from ground and Q_r (Figure 5e & 5f) were the smallest of any term for all synoptic types, with Q_g
424 and Q_r accounting for less than one percent of median daily energy fluxes for all synoptic types. Ground heat flux
425 characteristics were similar between all synoptic types and varied little. While Q_r was small when examined as a
426 daily median value, it does show a high degree of variation primarily associated with T5 and T3. This is due to
427 several large rain events that occurred during 2016 (18 July; 21 and 22 July; and 31 August) and one during 2017
428 (15 August). Despite relatively low energy flux contributions by rainfall, it is interesting to note that the ten days
429 with the highest rainfall fluxes ($>0.05 \text{ MJ m}^{-2} \text{ day}^{-1}$) consisted of four T5 days, three T3 days, two T7 days, and
430 one T6 day showing a significant clustering of high precipitation days in types T5 and T3.

431 3.2.4 Total daily net energy flux

432 Overall, two synoptic types (T5 and T6) had positive median daily net energy flux to the snowpack (Figure 6a).
433 Of these, T5 had the largest energy flux that was related to its relatively high temperatures that contributed to the
434 highest Q_h value of any synoptic type and increased solar radiation from less cloud cover. Contrary to the reduction
435 in cloud cover that aided T5 in having the highest total energy flux contributions, T6 had the highest cloud cover
436 and yet had the second highest energy flux to the snowpack that was primarily due to increased incoming
437 longwave radiation. T7 was close to having neutral energy fluxes with a median value of only $-0.04 \text{ MJ m}^{-2} \text{ day}^{-1}$
438 as a result of relatively low percentage of cloud cover resulting in strongly negative L^* as well as the second
439 highest Q_h term of any type.

440 T1 and T4 showed the greatest negative median daily net energy flux of all synoptic types (Figure 6a), which
441 could be attributed to their negative L^* and to having low K^* terms. T3 has a similar net energy flux to T4, but is
442 negative primarily due to having the only negative Q_h of any type. T2 also had a net negative median daily energy
443 flux but to a lesser extent than either T1, T3, or T4. Relative humidity values lower than any other type were the
444 primary driver behind T2's negative net value as it resulted in the highest longwave radiation loss from the
445 snowpack through having the lowest cloud cover, as well as Q_e loss.

446 The synoptic type T5 contributed the most energy to the snowpack during the two seasons (Figure 6b) due to a
447 moderate number of occurrences (22), an IQR that was higher than the other synoptic types, higher maximum
448 values, and having the largest positive fluxes from high Q_h values. Much of the energy flux of T5 was associated
449 with strong WAA ahead of the passage of cold fronts. While T6 was the only other type to have positive median
450 daily energy flux contributions to snowpack energy flux, T7 contributed a higher amount of energy flux during

451 the two winter periods. This occurred because it had the second highest number of occurrences, and the
452 distribution of occurrences around the median show that events were either near-neutral or positive in their energy
453 fluxes. T6 was the only other type to have a positive energy flux contribution to the snowpack over the two seasons
454 and it was smaller than that of T5 or T7. Similar magnitude was seen in the negative flux contributions of T1, T2,
455 and T4 with T2 having the most significant negative flux. T1 and T4 also showed negative fluxes, but T3 showed
456 a nearly neutral contribution to snowpack energy flux over the two winter seasons. As T3 is associated with a
457 surface trough, it's possible that pre-frontal and post-frontal characteristics are both incorporated in the energy
458 balance of T3 and act to cancel each other out when averaged over a longer period.

459 All synoptic types had variation in median daily net energy that can be attributed to the classification conducted
460 by the k-means clustering technique. Each type consisted of classified days that had similar synoptic
461 characteristics, but differences in system strength and position affected energy fluxes for individual days.
462 Therefore, it is important to remember that each synoptic type is associated with a range of daily energy flux
463 values in addition to the median daily energy flux for each type.

464 **3.2.5 Energy balance closure**

465 Daily site energy balance closure was determined by calculating snow water equivalent (SWE) from automated
466 snow depth measurements and median snowpack density and comparing the energy flux required for measured
467 decreases in SWE to the Q_{res} value for the same period. Closure was calculated for days where 50% or more
468 daytime periods had snowmelt and outliers were removed. A drawback of this method is that it does not distinguish
469 between types of ablation (melt, evaporation/sublimation, wind-scour) and any removal of snow through a process
470 other than melt will result in higher error in calculation of closure. Evaporation/sublimation is already included in
471 the calculation of energy balance closure as it is represented by measured latent heat flux. Therefore, the only
472 process that needs to be acknowledged as a potential source of snow removal in addition to melt when interpreting
473 the results of the closure calculations is wind-scour.

474 Mean energy balance closure for all periods and synoptic types was 0.62 ± 0.72 and, as Q_{ec} is a measure of error
475 in energy balance closure, it represented approximately 38% of total fluxes during the study. T4 had the only
476 negative closure (-0.24 ± 0.30) (Table 3) that was likely the result of strong winds scouring fresh snow from T3,
477 however, only one day of analysis existed for T4 and the results may not be applicable to the broader number of
478 days. T6 had the highest closure of any type (0.92 ± 1.13), but also showed one of the largest variations in closure
479 with only T2 (0.83 ± 1.33) having a larger standard deviation. Overall, mean values of wind speed and energy
480 balance closure of each synoptic type showed significant correlation ($r = -0.73, R^2 = 0.54$), suggesting that
481 wind-scour of the snowpack did have an impact on the calculation of energy balance closure.

482 **4 Discussion**

483 **4.1 Properties of synoptic type energy balance**

484 Net shortwave radiation flux contributed the largest amount of energy to the snowpack for all synoptic types
485 ranging from 53-97% of median daily energy flux with T5 being the only synoptic type below 60% contribution
486 (53%) of K^* to the snowpack. These results agree with Fayad et al. (2017) who noted that radiative fluxes are the
487 dominant source of snowpack melt energy in mountain ranges with Mediterranean climates. Net Q_h contributed
488 the second highest percentage of median daily energy flux to the snowpack accounting for 16-44% of positive

489 fluxes with the exception of T3 that had a Q_h term that accounted for 4% of its negative fluxes. The largest
490 contributions of Q_h to the snowpack are associated with synoptic types T2, T4, T5, and T7 that are characterised
491 by high pressure and northwesterly or westerly winds that are associated with WAA. Hay and Fitzharris (1988)
492 noted that, while radiative terms were responsible for the majority of energy contributions to glacier melt in New
493 Zealand's Southern Alps, turbulent fluxes contributed significant amounts of energy to melt. Similarly, despite
494 Q_h not being the dominant energy flux to the snowpack for any synoptic type, it does account for nearly half of
495 the energy flux to the snowpack for T5 (44%) and over a third for T7 (35%), and is still a significant source of
496 energy flux to the snowpack for nearly all synoptic types.

497 Median daily energy loss from the snowpack was from Q_e and Q^* , which dominated T1, T2, and T4 resulting in
498 negative median daily energy fluxes from the snowpack. Net longwave radiation was the most influential term in
499 the emission of energy from the snowpack accounting for 61-95% of energy loss with net Q_e flux accounting for
500 5-39% of outgoing energy flux. Though the methodology of this paper distinguishes between shortwave and
501 longwave fluxes in order to better examine the effects of synoptic-scale features such as RH or cloud cover on
502 radiative transfers similar to that of more recent works such as Cullen and Conway (2015), many historical works
503 have not made the same distinction in terms (Moore and Owens, 1984; Hay and Fitzharris, 1988; Neale and
504 Fitzharris, 1997; Stoy et al., 2018). It should be noted that had Q^* been used for comparison, the results of this
505 paper agree with several studies (Sade et al., 2014; Moore and Owens, 1984; Bednorz, 2008b) that found that
506 turbulent fluxes were the dominant fluxes when examining the energy flux characteristics on snowpacks in
507 climates similar to that of the Snowy Mountains in the Australian Alps.

508 Median daily Q_g values were found to account for only a small fraction of total energy flux to the snowpack
509 consisting of 1-5% of daily positive energy fluxes. Similarly, energy flux to the snowpack from Q_r has been
510 shown to only contribute < 1% of total seasonal energy flux for five of the seven synoptic types which agrees with
511 the findings of other studies (Bilish et al., 2018; Mazurkiewicz et al., 2008). However, precipitation was
512 responsible for > 1% of the daily median energy flux of the two synoptic types primarily associated with rain-on-
513 snow events, T5 and T3. Although fluxes imparted on the snowpack from rainfall are relatively small when
514 compared to all positive fluxes, the accompanying energy flux characteristics of T5 associated with rain-on-snow
515 events are responsible for two of the three largest contributions of overall snowpack energy fluxes.

516 The results show a significant agreement with previous research conducted in this region by Bilish et al. (2018)
517 when methods from that work are used to calculate relative contributions of positive energy fluxes to the
518 snowpack. Overall, incoming longwave radiation was shown to be the highest positive flux to the snowpack
519 accounting for 75-86% of incoming energy flux. Shortwave radiation was responsible for an additional 8-14% of
520 incoming energy flux with Q_h accounting for 0-9% of incoming fluxes, Q_e generating 0-4%, Q_g attributing 0.3%,
521 and Q_r accounting for 0.1%. Despite methodological differences that can be attributed to the need to highlight
522 different processes within atmosphere – snowpack interaction, results from both papers show similar overall
523 energy fluxes.

524 Energy balance closure at the site was similar to other research into snowpack energy balance (Welch et al., 2016)
525 and total error in closure was 38% during the entirety of the study. Though the method used to calculate energy
526 balance closure offered a good approximation, wind-scour is a significant source of error with this method.

527 Therefore, energy balance closure methods that incorporate internal measurements of snowpack energy are
528 preferable when possible.

529 **4.2 Synoptic patterns and energy flux**

530 Snowpack energy flux characteristics recorded at the Pipers Creek catchment headwaters have been related to
531 synoptic weather types that occurred during the 2016 and 2017 snow seasons. The resulting analysis reveals a
532 maximum in positive energy flux as pre-frontal troughs approach the Snowy Mountains, followed by cold front
533 conditions during the T7→T5→T3 common progression pattern identified here. Several factors cause high
534 positive energy flux during these periods that include: an increase in temperatures due to WAA and the associated
535 increase in positive Q_h ; decrease in negative L^* due to an increase in cloud cover; a decrease in Q_e following
536 frontal passage and associated increase in RH; and progressively increasing Q_r as the trough approaches and
537 immediately after passage.

538 Synoptic types characterized by surface high pressure as their primary influence (T1, T2, T4, and T7) had four of
539 the five negative daily contributions to snowpack energy flux. In T1 and T7, net shortwave radiation terms (K^*)
540 were positive and varied by ~4-10% for these types, however, low RH and cloud cover allowed for highly negative
541 L^* terms that were not compensated by change in K^* . In contrast, T4 had higher cloud cover and increased RH
542 that were due to advection of moisture from the Tasman Sea. The higher RH in T4 and low mean air temperature
543 (-2.06°C) resulted in Q_e and Q_h terms of similar magnitudes, but opposite signs that nearly cancelled out. This
544 resulted in a L^* term that was of lesser magnitude than those of T1, T2, and T7, but still the dominant term in its
545 energy exchange.

546 Four primary synoptic circulation patterns were identified during the study period. Each of the four patterns and
547 their associated energy flux values calculated from median daily flux and mean type duration can be seen in
548 Figures 4a and 4b. While each pattern differs towards the end of the cycle, each one has the T7→T5→T3
549 progression in common. Unsurprisingly, the highest contribution of median energy flux to the snowpack (0.75 MJ
550 m⁻²) is from Pattern 1, which has only two synoptic types with negative flux (T3 and T7) whereas the others all
551 contain three or four negative flux types. Pattern 3 had the largest negative snowpack energy flux (-2.44 MJ m⁻²)
552 due to it containing types with the highest net energy loss (T1 and T4).

553 Changing synoptic regimes in the Snowy Mountains suggest an increase in anti-cyclonic conditions (Hendon et
554 al., 2007;Pepler et al., 2019), such as types T1, T2, T4, and T7, as a result of poleward shift in the subtropical
555 ridge (Cai et al., 2005). Under these conditions, snowpack energy exchange in the Australian Alps would be
556 expected to decrease as synoptic types related to anti-cyclonic conditions have negative energy fluxes to the
557 snowpack. While these results may seem counterintuitive regarding a generally warming climate, they agree with
558 the findings of Theobald et al. (2016) who showed reductions in cool-season precipitation amounts and frequency
559 due, in part, to reductions in the occurrence of dominant cold front systems. The reduction in cold-frontal systems
560 in the Australian Alps region is associated with declines in the pre-frontal WAA that has been shown to be the
561 primary driver of positive snowpack energy flux. However, potential reductions in energy fluxes to the snowpack
562 will not likely lead to increases in snowpack duration or depth, as reductions in precipitation are associated with
563 the shifts to anti-cyclonic synoptic patterns (Theobald et al., 2016;Theobald et al., 2015).

564 The synoptic effects on snowpack energy balance identified in this paper represent those experienced within the
565 Pipers Creek catchment headwaters and are an important first step towards a more comprehensive understanding
566 of synoptic influences on the energy balance of the Snowy Mountains snowpack. As synoptic-scale effects on the
567 wider region likely differ from those described here, caution should be exercised before upscaling the Pipers Creek
568 catchment headwaters measurements to the broader Snowy Mountains region. Pomeroy et al. (2003) noted that
569 differing slope and aspect of three proximal energy balance sites showed significant control on whether daily net
570 radiation was positive or negative and that daily incoming solar radiation varied by as much as 26% as a result.
571 Similar effects of complex terrain on turbulent fluxes exist, as terrain-induced flows will contribute to
572 measurements of turbulent fluxes in addition to measured effects of synoptic patterns. Therefore, consideration of
573 an area's slope, aspect, and surrounding terrain is crucial to understanding synoptic-scale effects on its energy
574 balance.

575 **4.3 Distribution of gap-filled eddy covariance fluxes**

576 One of the disadvantages of the Random Forest regression method to gap-fill missing EC data is that exact results
577 aren't reproducible due to the method's random handling and sub-setting of predictor variables. Methods of
578 developing models and predicting values were evaluated over twenty iterations to determine the amount of
579 variability in RMSE when generating a random forest from the same dataset. Some variability in RMSE was noted
580 between tests for Q_e and Q_h but was small with a standard deviation of 0.01 Wm^{-2} in Q_e and 0.03 Wm^{-2} in Q_h .
581 Small differences in RMSEs between model development runs and data filling indicate that RMSE values for gap-
582 filled data would be best represented as $2.56 \pm 0.01 \text{ Wm}^{-2}$ for Q_e and $4.67 \pm 0.03 \text{ Wm}^{-2}$ for Q_h

583 Gap-filling of Q_h and Q_e can introduce uncertainty into measurements that may affect the ability to thoroughly
584 compare datasets such as those pertaining to the different synoptic types compared within this work. As such, it
585 is important to note that not all synoptic types had equal amounts of gap-filling for their Q_e and Q_h fluxes.
586 Distribution of gap-filled data within synoptic types depended largely on the quantity of precipitation associated
587 with each type. The most significant concentrations of gap-filled data were in T3 (Q_e : 74%, Q_h : 55%) T5 (Q_e :
588 57%, Q_h : 39%), and T6 (Q_e : 81%, Q_h : 73%). Differences in the quantity of gap-filled data between synoptic types
589 can create uncertainty when making comparisons between fluxes in each. However, uncertainty introduced
590 through gap-filling procedures is relatively low and should have a minimal impact during comparison of fluxes.

591 **5 Conclusions**

592 Overall, periods of pre-cold frontal passage contribute the most energy fluxes to snowpack melt due to WAA
593 ahead of the front, a reduction in cloud cover allowing for higher incoming shortwave radiation, and the gradual
594 development of precipitation that often contributes to rain-on-snow events. While this work was conducted solely
595 on the Australian snowpack, snowpacks in other regions such as New Zealand (Hay and Fitzharris, 1988; Neale
596 and Fitzharris, 1997), Canada (Romolo et al., 2006a; 2006b), the Spanish Pyrenees (Lopez-Moreno and Vicente-
597 Serrano, 2007), and the Arctic (Drobot and Anderson, 2001) see similar synoptic-scale effects on snowpack
598 energy to those presented here. Snowpack energy fluxes in the Australian Alps would likely decrease under
599 climate change progression as a result of reductions to primary cold-frontal systems and associated pre-frontal
600 WAA. However, as this study developed relationships between synoptic patterns and snowpack energy fluxes
601 based on single-site measurements in the Pipers Creek catchment headwaters, their applicability may be limited
602 and caution should be exercised before applying them to the broader region.

603 The understanding of synoptic-scale processes on snowpack energy balances will likely become applicable to
604 broader regions as climate change continues and snowpacks develop warmer properties (Stewart, 2009;Adam et
605 al., 2009;Pepler et al., 2019;Catto et al., 2014;Cai et al., 2005;Theobald et al., 2016;Chubb et al., 2011). An
606 increased burden on freshwater systems for agriculture, drinking water, and energy production will continue as
607 these changes occur (Parry et al., 2007). Therefore, continued work on marginal snowpack ablation processes,
608 such as those within the forested regions of Australia’s Snowy Mountains, will be important to resource
609 management and should be explored.

610 **Data Availability**

611 Energy flux data used in this study is available at <https://doi.org/10.14264/uql.2019.691>. ERA-Interim reanalysis
612 data are freely available from the European Centre for Medium-Range Weather Forecasts
613 (<https://www.ecmwf.int/en/forecasts/datasets/reanalysis-datasets/era-interim>). Precipitation data used in this
614 study was supplied by Snowy Hydro Limited via restricted access, this data can be obtained by contacting Snowy
615 Hydro Ltd.

616 **Author Contributions**

617 AS, HM, AT, and NC designed the experiments and AS conducted them. AT developed the k-means clustering
618 and synoptic typing code. AS developed the code related to energy balance and eddy covariance measurements.
619 AS wrote the manuscript with input from all authors.

620 **Competing Interests**

621 The authors declare that they have no competing interests.

622 **Acknowledgements**

623 The authors would like to thank Shane Bilish for establishment of the Pipers Creek snowpack research catchment,
624 Michael Gray for installation and maintenance of the energy balance tower, and the Weather and Water team at
625 Snowy Hydro Limited for their contributions of data and field support during the data collection and analysis
626 process. AS was supported by an Australian Government Research Training Program Scholarship.

627

628

629

630

631 **References**

- 632 Adam, J. C., Hamlet, A. F., and Lettenmaier, D. P.: Implications of global climate change for snowmelt hydrology
633 in the twenty-first century, *Hydrological Processes: An International Journal*, 23, 962-972, 2009.
- 634 Ahrens, C. D.: *Meteorology today: an introduction to weather, climate, and the environment*, Cengage Learning,
635 2012.
- 636 Allan, R. P., Shine, K. P., Slingo, A., and Pamment, J.: The dependence of clear-sky outgoing long-wave radiation
637 on surface temperature and relative humidity, *Quarterly Journal of the Royal Meteorological Society*
638 125, 2103-2126, 1999.
- 639 Australian Bureau of Statistics, Water Use on Australian Farms, 2018-19:
640 <https://www.abs.gov.au/ausstats/abs@.nsf/mf/4618.0>, access: June 4, 2020.
- 641 Bednorz, E.: Synoptic conditions of snow occurrence in Budapest, *Meteorologische Zeitschrift*, 17, 39-45,
642 10.1127/0941-2948/2008/0262, 2008a.
- 643 Bednorz, E.: Synoptic reasons for heavy snowfalls in the Polish–German lowlands, 92, 133-140, 2008b.
- 644 Bednorz, E.: Synoptic conditions of the occurrence of snow cover in central European lowlands, 31, 1108-1118,
645 2011.
- 646 Beniston, M.: Climatic Change in Mountain Regions: A Review of Possible Impacts, *Climatic Change*, 59, 5-31,
647 10.1023/a:1024458411589, 2003.
- 648 Bilish, S. P., McGowan, H. A., and Callow, J. N.: Energy balance and snowmelt drivers of a marginal subalpine
649 snowpack, *Hydrol Process*, 32, 3837-3851, 2018.
- 650 Bilish, S. P., Callow, J. N., McGrath, G. S., and McGowan, H. A.: Spatial controls on the distribution and
651 dynamics of a marginal snowpack in the Australian Alps, *Hydrol Process*, 33, 1739-1755, 10.1002/hyp.13435,
652 2019.
- 653 Bormann, K. J., Westra, S., Evans, J. P., and McCabe, M. F.: Spatial and temporal variability in seasonal snow
654 density, *J Hydrol*, 484, 63-73, 2013.
- 655 Breiman, L.: Random Forests, *Machine Learning*, 45, 5-32, 10.1023/a:1010933404324, 2001.
- 656 Budin, G.: Interannual variability of Australian snowfall, *Aust. Met. Mag.*, 33, 145-159, 1985.
- 657 BOM: Analysis Chart Archive: <http://www.bom.gov.au/australia/charts/archive/>, access: 15.09.2018, 2018a.
- 658 BOM: Climate Statistics for Australian Locations: <http://www.bom.gov.au/climate/data/>, access: 13.12.2018,
659 2018b.

660 Burles, K., and Boon, S.: Snowmelt energy balance in a burned forest plot, Crowsnest Pass, Alberta, Canada,
661 Hydrol Process, 25, 3012-3029, 10.1002/hyp.8067, 2011.

662 Cai, W., Shi, G., Cowan, T., Bi, D., and Ribbe, J.: The response of the Southern Annular Mode, the East Australian
663 Current, and the southern mid-latitude ocean circulation to global warming, 32, doi:10.1029/2005GL024701,
664 2005.

665 Callow, N., McGowan, H., Warren, L., and Speirs, J.: Drivers of precipitation stable oxygen isotope variability in
666 an alpine setting, Snowy Mountains, Australia, Journal of Geophysical Research: Atmospheres, 119, 3016-3031,
667 10.1002/2013JD020710, 2014.

668 Campbell Scientific EC150 CO₂/H₂O Open-Path Gas Analyzer: <https://www.campbellsci.com/manuals>, access:
669 24.10.2018, 2018.

670 Catto, J. L., Nicholls, N., Jakob, C., and Shelton, K. L.: Atmospheric fronts in current and future climates, Geophys
671 Res Lett, 41, 7642-7650, 10.1002/2014gl061943, 2014.

672 Chubb, T. H., Siems, S. T., and Manton, M. J.: On the Decline of Wintertime Precipitation in the Snowy
673 Mountains of Southeastern Australia, J Hydrometeorol, 12, 1483-1497, 10.1175/Jhm-D-10-05021.1, 2011.

674 Costin, A. B., and Gay, D.: Studies in Catchment Hydrology in the Australian Alps, MPKV; Maharastra, 1961.

675 Cullen, N. J., and Conway, J. P.: A 22 month record of surface meteorology and energy balance from the ablation
676 zone of Brewster Glacier, New Zealand, J Glaciol, 61, 931-946, 2015.

677 Dee, D. P., Uppala, S. M., Simmons, A., Berrisford, P., Poli, P., Kobayashi, S., Andrae, U., Balmaseda, M.,
678 Balsamo, G., and Bauer, d. P.: The ERA-Interim reanalysis: Configuration and performance of the data
679 assimilation system, Quarterly Journal of the royal meteorological society, 137, 553-597, 2011.

680 Di Luca, A., Evans, J. P., and Ji, F.: Australian snowpack in the NARClIM ensemble: evaluation, bias correction
681 and future projections, Climate Dynamics, 51, 639-666, 10.1007/s00382-017-3946-9, 2018.

682 Drobot, S. D., and Anderson, M. R.: Comparison of interannual snowmelt-onset dates with atmospheric
683 conditions, Annals of Glaciology, 33, 79-84, 2001.

684 Duus, A. L.: Estimation and analysis of snow cover in the Snowy Mountains between 1910 and 1991, Aust
685 Meteorol Mag, 40, 195-204, 1992.

686 Ellis, C. R., Pomeroy, J. W., Essery, R. L. H., and Link, T. E.: Effects of needleleaf forest cover on radiation and
687 snowmelt dynamics in the Canadian Rocky Mountains, Can J Forest Res, 41, 608-620, 10.1139/X10-227, 2011.

688 Falge, E., Baldocchi, D., Olson, R., Anthoni, P., Aubinet, M., Bernhofer, C., Burba, G., Ceulemans, G., Clement,
689 R., Dolman, H., Granier, A., Gross, P., Grunwald, T., Hollinger, D., Jensen, N. O., Katul, G., Keronen, P.,
690 Kowalski, A., Lai, C. T., Law, B. E., Meyers, T., Moncrieff, J., Moors, E., Munger, J. W., Pilegaard, K., Rannik,

691 U., Rebmann, C., Suyker, A., Tenhunen, J., Tu, K., Verma, S., Vesala, T., Wilson, K., and Wofsy, S.: Gap filling
692 strategies for long term energy flux data sets, *Agr Forest Meteorol*, 107, 71-77, Doi 10.1016/S0168-
693 1923(00)00235-5, 2001a.

694 Falge, E., Baldocchi, D., Olson, R., Anthoni, P., Aubinet, M., Bernhofer, C., Burba, G., Ceulemans, R., Clement,
695 R., Dolman, H., Granier, A., Gross, P., Grunwald, T., Hollinger, D., Jensen, N. O., Katul, G., Keronen, P.,
696 Kowalski, A., Lai, C. T., Law, B. E., Meyers, T., Moncrieff, H., Moors, E., Munger, J. W., Pilegaard, K., Rannik,
697 U., Rebmann, C., Suyker, A., Tenhunen, J., Tu, K., Verma, S., Vesala, T., Wilson, K., and Wofsy, S.: Gap filling
698 strategies for defensible annual sums of net ecosystem exchange, *Agr Forest Meteorol*, 107, 43-69, Doi
699 10.1016/S0168-1923(00)00225-2, 2001b.

700 Fayad, A., Gascoïn, S., Faour, G., López-Moreno, J. I., Drapeau, L., Le Page, M., and Escadafal, R.: Snow
701 hydrology in Mediterranean mountain regions: A review, *J Hydrol*, 551, 374-396, 2017.

702 Fiddes, S. L., Pezza, A. B., and Barras, V.: A new perspective on Australian snow, *Atmospheric Science Letters*,
703 16, 246-252, 10.1002/asl2.549, 2015a.

704 Fiddes, S. L., Pezza, A. B., and Barras, V.: Synoptic climatology of extreme precipitation in alpine Australia,
705 *International Journal of Climatology*, 35, 172-188, 2015b.

706 Gellie, N. J. H.: Native vegetation of the Southern Forests: South-east highlands, Australian alps, south-west
707 slopes and SE corner bioregions, Royal Botanic Gardens, 2005.

708 Goree, P. A., and Younkin, R. J.: Synoptic Climatology of Heavy Snowfall Over the Central and Eastern United
709 States, 94, 663-668, 10.1175/1520-0493(1966)094<0663:Scohso>2.3.Co;2, 1966.

710 Granger, R. J., and Gray, D. M.: A Net-Radiation Model for Calculating Daily Snowmelt in Open Environments,
711 *Nord Hydrol*, 21, 217-234, 1990.

712 Gray, M. A., McGowan, H. A., Lowry, A. L., and Guyot, A.: Surface energy exchanges over contrasting
713 vegetation types on a sub-tropical sand island, *Agr Forest Meteorol*, 249, 81-99, 10.1016/j.agrformet.2017.11.018,
714 2018.

715 Grundstein, A. J., and Leathers, D. J.: A case study of the synoptic patterns influencing midwinter snowmelt
716 across the northern Great Plains, 12, 2293-2305, doi:10.1002/(SICI)1099-1085(199812)12:15<2293::AID-
717 HYP797>3.0.CO;2-9, 1998.

718 Hay, J. E., and Fitzharris, B. B.: The synoptic climatology of ablation on a New Zealand glacier, *Journal of*
719 *Climatology*, 8, 201-215, 10.1002/joc.3370080207, 1988.

720 Helgason, W., and Pomeroy, J.: Problems Closing the Energy Balance over a Homogeneous Snow Cover during
721 Midwinter, *J Hydrometeorol*, 13, 557-572, 10.1175/Jhm-D-11-0135.1, 2012.

722 Hendon, H. H., Thompson, D. W. J., and Wheeler, M. C.: Australian Rainfall and Surface Temperature Variations
723 Associated with the Southern Hemisphere Annular Mode, 20, 2452-2467, 10.1175/jcli4134.1, 2007.

724 Hennessy, K. J., Whetton, P. H., Walsh, K., Smith, I. N., Bathols, J. M., Hutchinson, M., and Sharples, J.: Climate
725 change effects on snow conditions in mainland Australia and adaptation at ski resorts through snowmaking, *Clim*
726 *Res*, 35, 255-270, 10.3354/cr00706, 2008.

727 Kidson, J. W.: An analysis of New Zealand synoptic types and their use in defining weather regimes, *International*
728 *journal of climatology*, 20, 299-316, 2000.

729 Liaw, A., and Wiener, M.: Classification and Regression by randomForest, *R News*, 2, 18-22, 2002.

730 Lopez-Moreno, J. I., and Vicente-Serrano, S. M.: Atmospheric circulation influence on the interannual variability
731 of snow pack in the Spanish Pyrenees during the second half of the 20th century, *Nord Hydrol*, 38, 33-44,
732 10.2166/nh.2007.030, 2007.

733 Male, D. H., and Granger, R. J.: Snow Surface-Energy Exchange, *Water Resour Res*, 17, 609-627, DOI
734 10.1029/WR017i003p00609, 1981.

735 Marks, D., and Dozier, J.: Climate and Energy Exchange at the Snow Surface in the Alpine Region of the Sierra-
736 Nevada .2. Snow Cover Energy-Balance, *Water Resour Res*, 28, 3043-3054, Doi 10.1029/92wr01483, 1992.

737 Mauder, M., and Foken, T.: Documentation and instruction manual of the eddy-covariance software package TK3,
738 2011.

739 Mazurkiewicz, A. B., Callery, D. G., and McDonnell, J. J.: Assessing the controls of the snow energy balance and
740 water available for runoff in a rain-on-snow environment, *J Hydrol*, 354, 1-14, 2008.

741 McGregor, G. R., and Gellatly, A. F.: The Energy Balance of a Melting Snowpack in the French Pyrenees During
742 Warm Anticyclonic Conditions, *International Journal of Climatology: A Journal of the Royal Meteorological*
743 *Society*, 16, 479-486, doi:10.1002/(SICI)1097-0088(199604)16:4<479::AID-JOC17>3.0.CO;2-W, 1996.

744 McKay, D. C., and Thurtell, G. W.: Measurements of the energy fluxes involved in the energy budget of a snow
745 cover, *J Appl Meteorol*, 17, 339-349, 1978.

746 Michelson, D. B.: Systematic correction of precipitation gauge observations using analyzed meteorological
747 variables, *J Hydrol*, 290, 161-177, 2004.

748 Moore, R., and Owens, I.: Controls on advective snowmelt in a maritime alpine basin, *Journal of Climate and*
749 *Applied Meteorology*

750 23, 135-142, 1984.

751 Neale, S. M., and Fitzharris, B. B.: Energy balance and synoptic climatology of a melting snowpack in the
752 Southern Alps, New Zealand, *International Journal of Climatology*, 17, 1595-1609, 10.1002/(SICI)1097-
753 0088(19971130)17:14<1595::AID-JOC213>3.0.CO;2-7, 1997.

754 Nicholls, N.: Climate variability, climate change and the Australian snow season, *Aust Meteorol Mag*, 54, 177-
755 185, 2005.

756 Pachauri, R. K., Allen, M. R., Barros, V. R., Broome, J., Cramer, W., Christ, R., Church, J. A., Clarke, L., Dahe,
757 Q., and Dasgupta, P.: Climate change 2014: synthesis report. Contribution of Working Groups I, II and III to the
758 fifth assessment report of the Intergovernmental Panel on Climate Change, IPCC, 2014.

759 Parry, M., Parry, M. L., Canziani, O., Palutikof, J., Van der Linden, P., and Hanson, C.: Climate change 2007-
760 impacts, adaptation and vulnerability: Working group II contribution to the fourth assessment report of the IPCC,
761 Cambridge University Press, 2007.

762 Pepler, A., Hope, P., and Dowdy, A.: Long-term changes in southern Australian anticyclones and their impacts
763 (vol 53, pg 4701, 2019), *Climate Dynamics*, 53, 4715-4715, 10.1007/s00382-019-04931-w, 2019.

764 Pepler, A. S., Trewin, B., and Ganter, C.: The influences of climate drivers on the Australian snow season, *Aust*
765 *Meteorol Ocean*, 65, 195-205, Doi 10.22499/2.6502.002, 2015.

766 Pomeroy, J. W., Toth, B., Granger, R. J., Hedstrom, N. R., and Essery, R. L. H.: Variation in surface energetics
767 during snowmelt in a subarctic mountain catchment, *J Hydrometeorol*, 4, 702-719, Doi 10.1175/1525-
768 7541(2003)004<0702:Viseds>2.0.Co;2, 2003.

769 Pook, M. J., McIntosh, P. C., and Meyers, G. A.: The synoptic decomposition of cool-season rainfall in the
770 southeastern Australian cropping region, *Journal of Applied Meteorology Climatology*, 45, 1156-1170, 2006.

771 Pook, M. J., Risbey, J., and McIntosh, P.: East coast lows, atmospheric blocking and rainfall: a Tasmanian
772 perspective, *IOP Conference Series: Earth and Environmental Science*, 2010, 012011,

773 Pook, M. J., Risbey, J. S., and McIntosh, P. C.: The synoptic climatology of cool-season rainfall in the central
774 wheatbelt of Western Australia, *Monthly Weather Review*, 140, 28-43, 2012.

775 Pook, M. J., Risbey, J. S., and McIntosh, P. C.: A comparative synoptic climatology of cool-season rainfall in
776 major grain-growing regions of southern Australia, *Theoretical Applied Climatology*, 117, 521-533,
777 10.1007/s00704-013-1021-y, 2014.

778 Prezerakos, N. G., and Angouridakis, V. E.: Synoptic consideration of snowfall in Athens, *Journal of Climatology*,
779 4, 269-285, 10.1002/joc.3370040305, 1984.

780 Rasmussen, R., Baker, B., Kochendorfer, J., Meyers, T., Landolt, S., Fischer, A. P., Black, J., Theriault, J. M.,
781 Kucera, P., Gochis, D., Smith, C., Nitu, R., Hall, M., Ikeda, K., and Gutmann, E.: How Well Are We Measuring

782 Snow? The NOAA/FAA/NCAR Winter Precipitation Test Bed, *B Am Meteorol Soc*, 93, 811-829, 10.1175/Bams-
783 D-11-00052.1, 2012.

784 Reba, M. L., Link, T. E., Marks, D., and Pomeroy, J.: An assessment of corrections for eddy covariance measured
785 turbulent fluxes over snow in mountain environments, *Water Resour Res*, 45, 10.1029/2008wr007045, 2009.

786 Reinfelds, I., Swanson, E., Cohen, T., Larsen, J., and Nolan, A.: Hydrospatial assessment of streamflow yields
787 and effects of climate change: Snowy Mountains, Australia, *J Hydrol*, 512, 206-220,
788 10.1016/j.jhydrol.2014.02.038, 2014.

789 Robock, A.: The seasonal cycle of snow cover, sea ice and surface albedo, *Monthly Weather Review*, 108, 267-
790 285, 1980.

791 Romolo, L., Prowse, T. D., Blair, D., Bonsal, B. R., Marsh, P., and Martz, L. W.: The synoptic climate controls
792 on hydrology in the upper reaches of the Peace River Basin. Part II: Snow ablation, 20, 4113-4129,
793 doi:10.1002/hyp.6422, 2006a.

794 Romolo, L., Prowse, T. D., Blair, D., Bonsal, B. R., and Martz, L. W.: The synoptic climate controls on hydrology
795 in the upper reaches of the Peace River Basin. Part I: snow accumulation, 20, 4097-4111, doi:10.1002/hyp.6421,
796 2006b.

797 Ruckstuhl, C., Philipona, R., Morland, J., and Ohmura, A.: Observed relationship between surface specific
798 humidity, integrated water vapor, and longwave downward radiation at different altitudes, *Journal of Geophysical*
799 *Research: Atmospheres*, 112, 2007.

800 Sade, R., Rimmer, A., Litaor, M. I., Shamir, E., and Furman, A.: Snow surface energy and mass balance in a warm
801 temperate climate mountain, *J Hydrol*, 519, 848-862, 2014.

802 Snowy Hydro Limited Snow Depths Calculator: [https://www.snowyhydro.com.au/our-
803 energy/water/inflows/snow-depths-calculator/](https://www.snowyhydro.com.au/our-energy/water/inflows/snow-depths-calculator/), access: 03/08/2018, 2018.

804 Stewart, I. T.: Changes in snowpack and snowmelt runoff for key mountain regions, *Hydrol Process*, 23, 78-94,
805 10.1002/hyp.7128, 2009.

806 Stiperski, I., and Rotach, M. W.: On the Measurement of Turbulence Over Complex Mountainous Terrain, *Bound-
807 Lay Meteorol*, 159, 97-121, 10.1007/s10546-015-0103-z, 2016.

808 Stoy, P. C., Peitzsch, E., Wood, D., Rottinghaus, D., Wohlfahrt, G., Goulden, M., and Ward, H.: On the exchange
809 of sensible and latent heat between the atmosphere and melting snow, *Agricultural Forest Meteorology*, 252, 167-
810 174, 2018.

811 Stull, R.: Wet-Bulb Temperature from Relative Humidity and Air Temperature, *J Appl Meteorol Clim*, 50, 2267-
812 2269, 10.1175/Jamc-D-11-0143.1, 2011.

813 Sturm, M., Holmgren, J., and Liston, G. E.: A seasonal snow cover classification system for local to global
814 applications, *J Climate*, 8, 1261-1283, 1995.

815 Theobald, A., McGowan, H., Speirs, J., and Callow, N.: A Synoptic Classification of Inflow-Generating
816 Precipitation in the Snowy Mountains, Australia, *J Appl Meteorol Clim*, 54, 1713-1732, 10.1175/Jamc-D-14-
817 0278.1, 2015.

818 Theobald, A., McGowan, H., and Speirs, J.: Trends in synoptic circulation and precipitation in the Snowy
819 Mountains region, Australia, in the period 1958-2012, *Atmos Res*, 169, 434-448, 10.1016/j.atmosres.2015.05.007,
820 2016.

821 Ueno, K.: Synoptic conditions causing nonmonsoon snowfalls in the Tibetan Plateau, *Geophys Res Lett*, 32, 2005.

822 Viviroli, D., Durr, H. H., Messerli, B., Meybeck, M., and Weingartner, R.: Mountains of the world, water towers
823 for humanity: Typology, mapping, and global significance, *Water Resour Res*, 43, Artn W07447
824 10.1029/2006wr005653, 2007.

825 Webb, E. K., Pearman, G. I., and Leuning, R.: Correction of flux measurements for density effects due to heat
826 and water vapour transfer, *Quarterly Journal of the Royal Meteorological Society*, 106, 85-100, 1980.

827 Webb, M., Slingol, A., and Stephens, G.: Seasonal variations of the clear-sky greenhouse effect: The role of
828 changes in atmospheric temperatures and humidities, *Climate dynamics*, 9, 117-129, 1993.

829 Welch, C. M., Stoy, P. C., Rains, F. A., Johnson, A. V., and McGlynn, B. L.: The impacts of mountain pine beetle
830 disturbance on the energy balance of snow during the melt period, *Hydrol Process*, 30, 588-602,
831 10.1002/hyp.10638, 2016.

832 Whetton, P. H., Haylock, M. R., and Galloway, R.: Climate change and snow-cover duration in the Australian
833 Alps, *Climatic Change*, 32, 447-479, Doi 10.1007/Bf00140356, 1996.

834 Wilks, D. S.: Cluster analysis, in: *International geophysics*, Elsevier, 603-616, 2011.

835

836

837

838

839

840

841

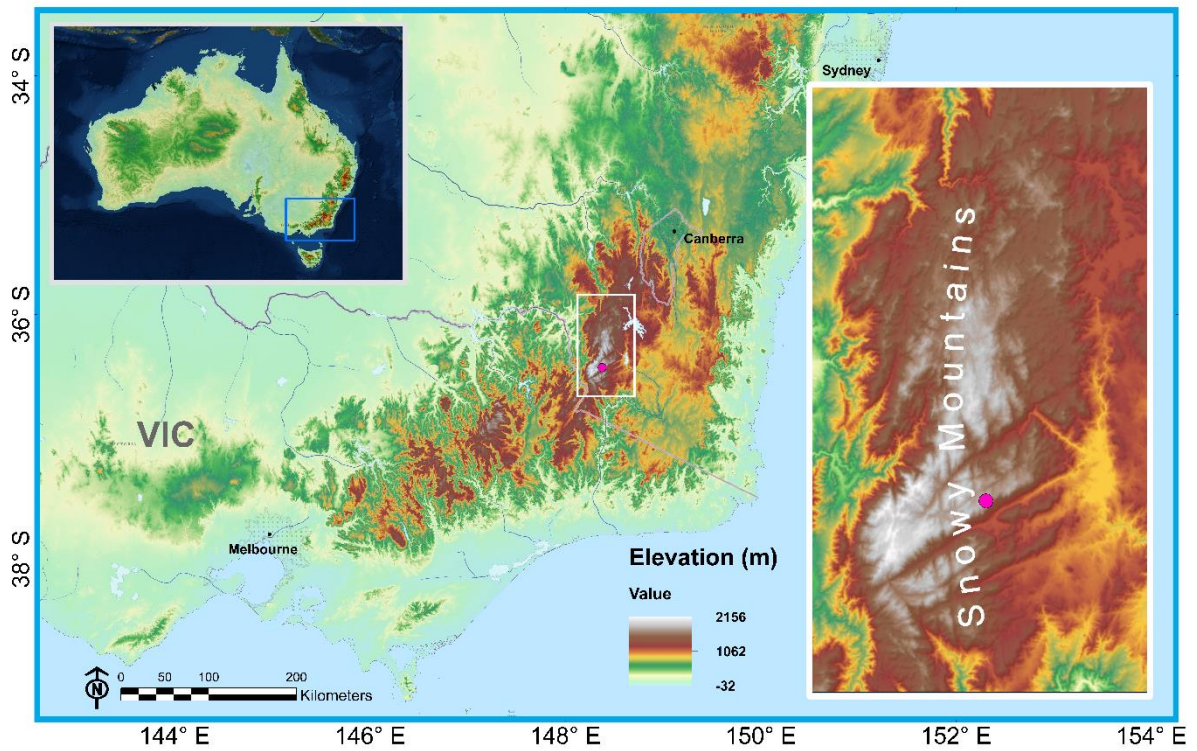
842

843

844

845

846
847
848
849
850
851
852
853



854 **Figure 1: Map of southeast Australia and the Snowy Mountains. Pink dot represents the location of the energy balance**
855 **instrumentation site. Map layer sources copyright: ESRI, USGS, NOAA, DigitalGlobe, GeoEye, Earthstar**
856 **Geographics, CNE S/A Airbus DS, USDA, AeroGRID, IGN, and the GIS User Community.**

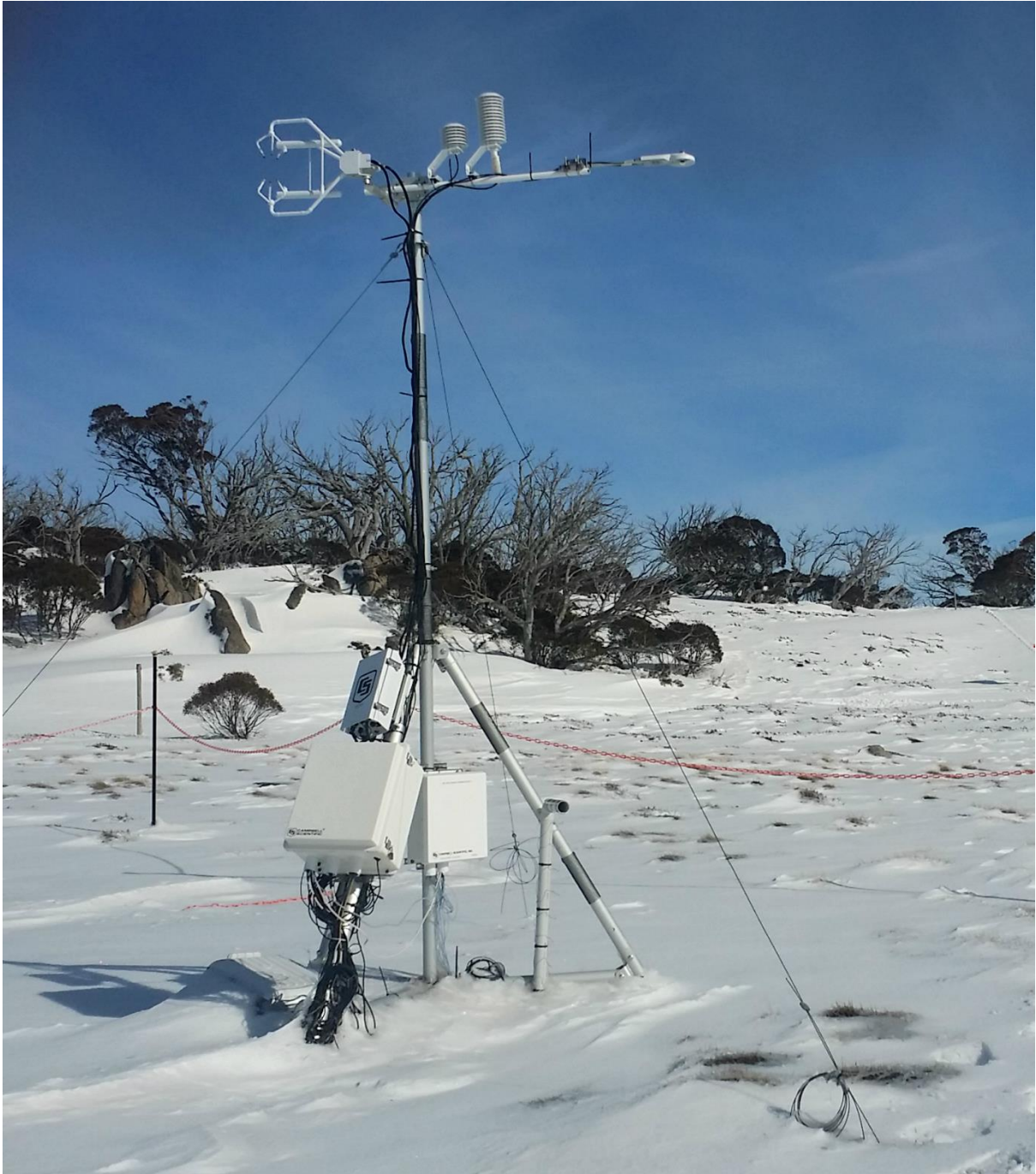
857
858
859
860
861

862

863

864

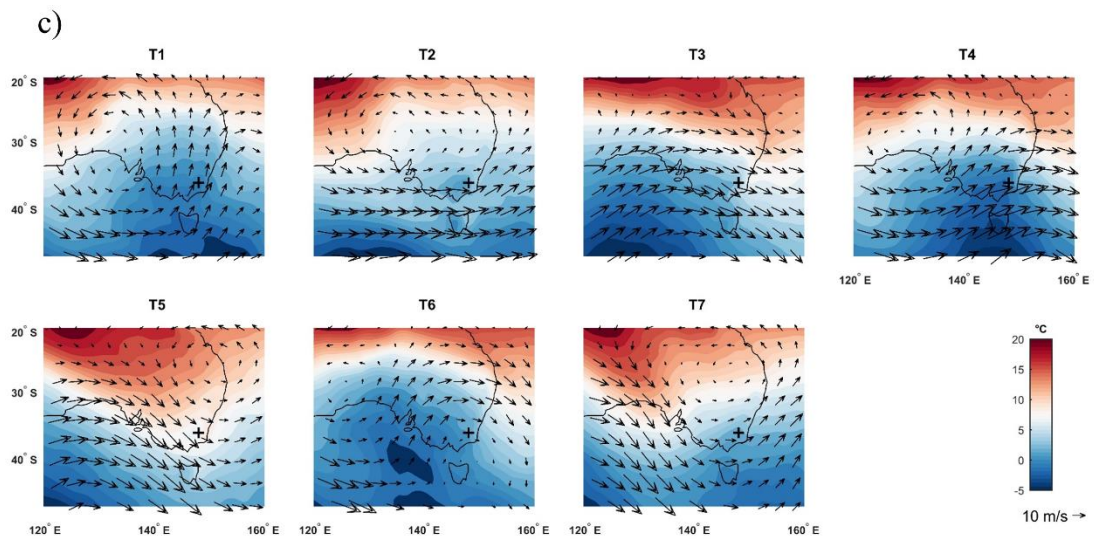
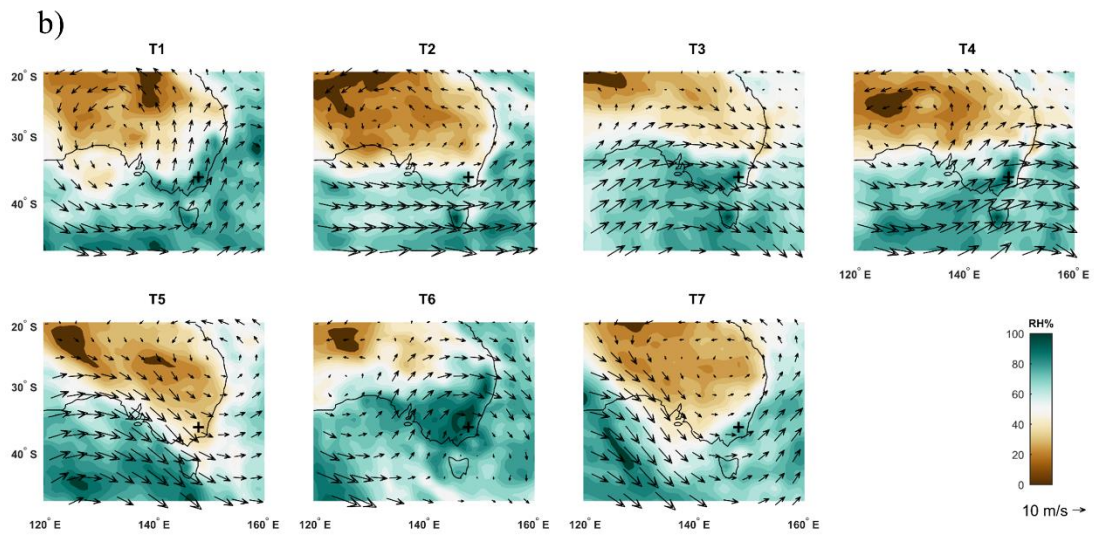
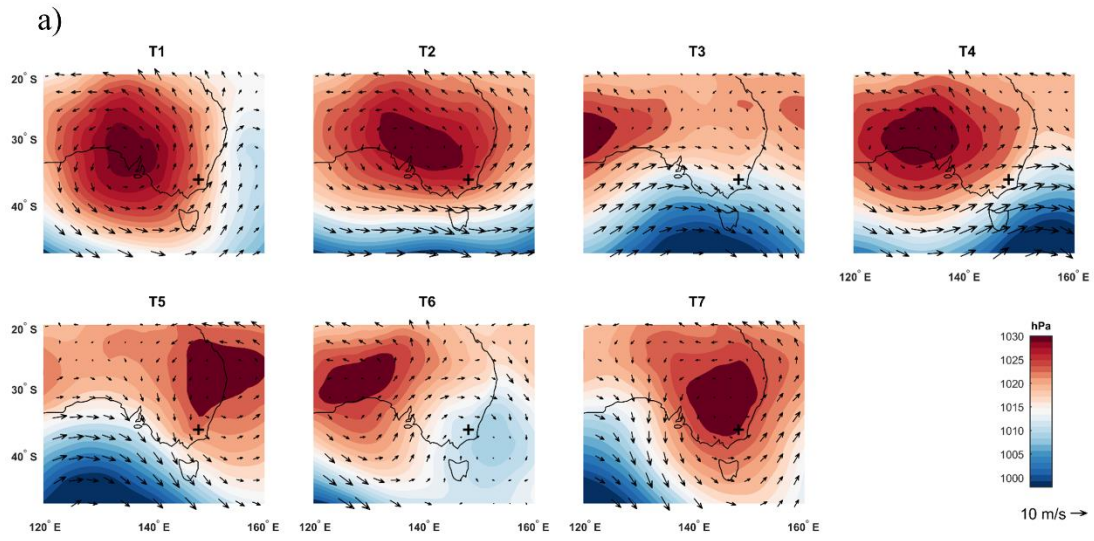
865



866

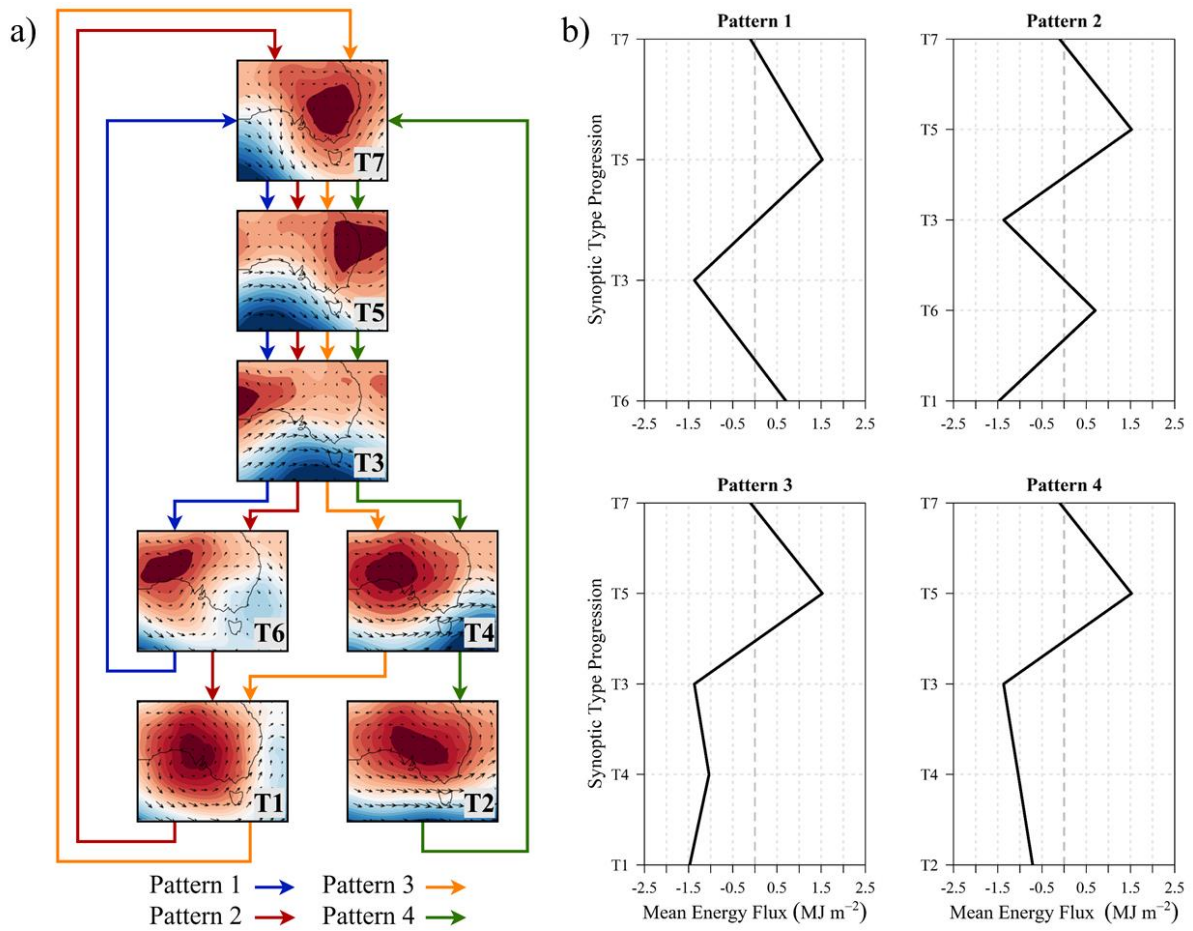
867

868 **Figure 2: Energy balance field site with eddy covariance instrumentation at Pipers Creek catchment headwaters.**



871 **Figure 3: Mean synoptic type MSLP and 10m wind vectors (a), 850 hPa RH and wind vectors (b), and 850 hPa T_d and**
872 **wind vectors (c) over the southeast Australia region for the 2016 and 2017 seasons. Location of surface energy balance**
873 **site marked with ‘+’.**

874



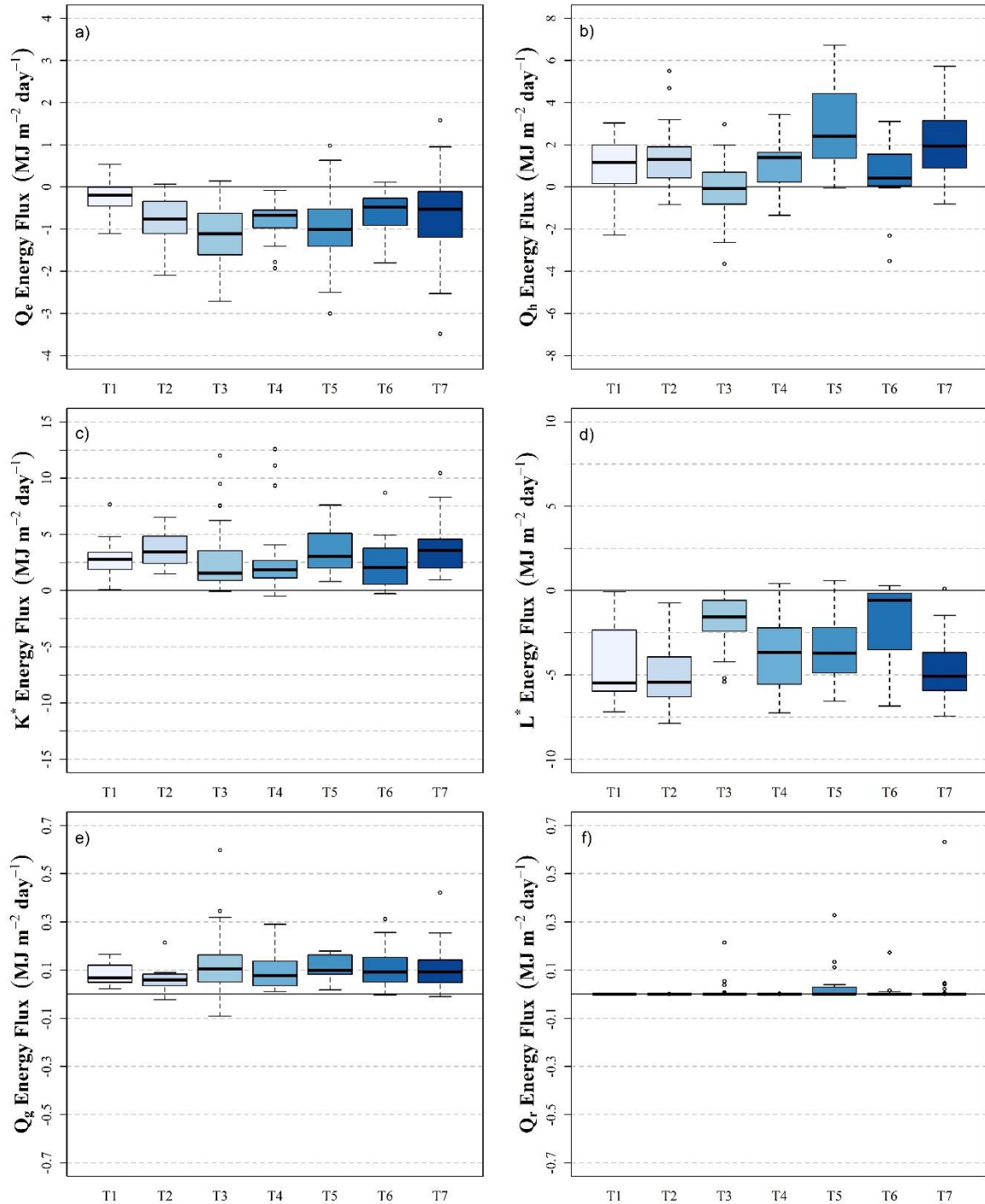
875

876 **Figure 4: Flowchart of four primary synoptic type patterns/progressions based on probability of transition for the 2016**
877 **and 2017 seasons (a) and calculated synoptic pattern snowpack fluxes based on median daily values and mean duration**
878 **of synoptic type (b).**

879

880

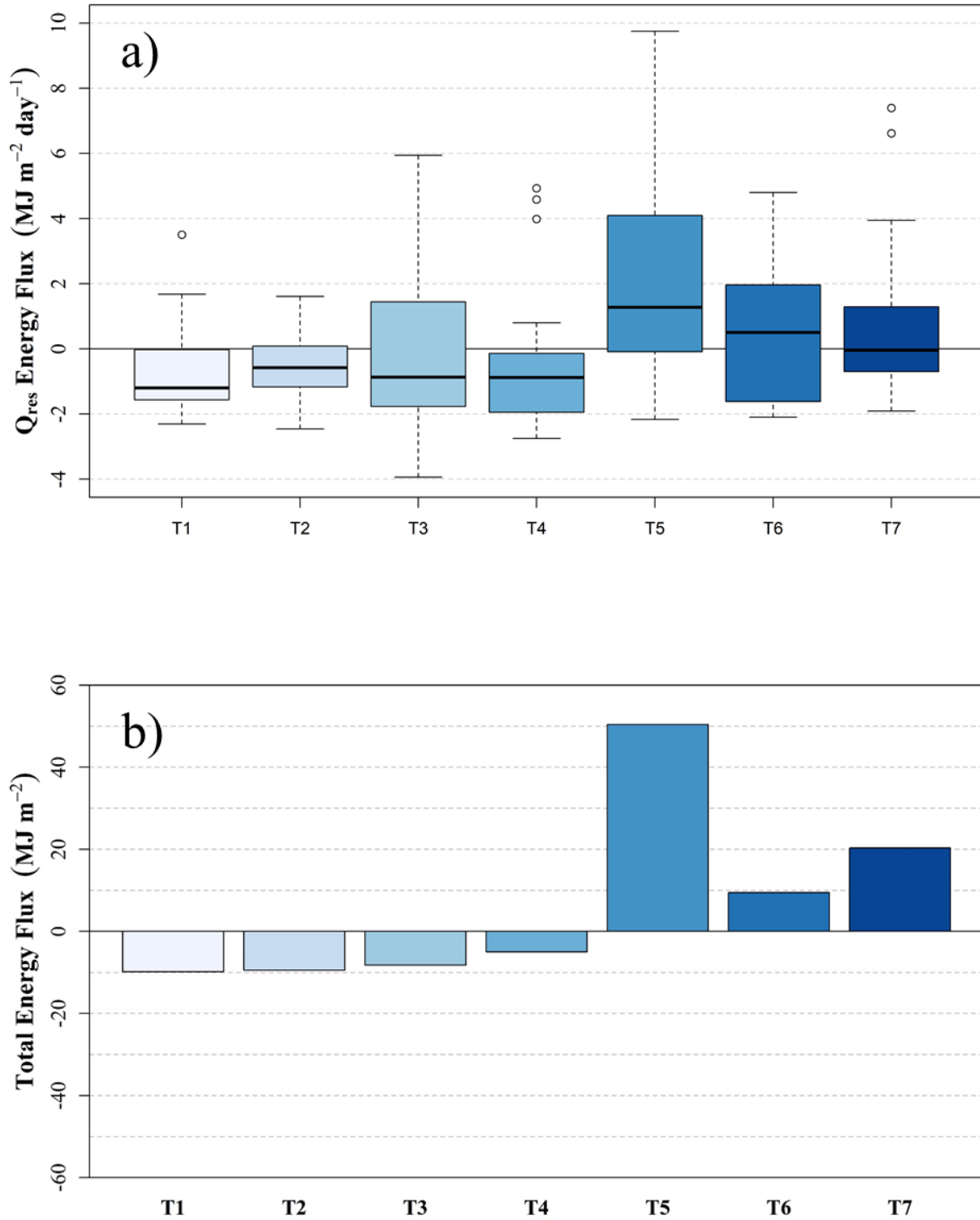
881
882
883



884 **Figure 5: Boxplots of daily snowpack latent heat (a), sensible heat (b), net shortwave radiation (c), net longwave**
885 **radiation (d), ground heat flux (e), and liquid precipitation (f) energy fluxes for each synoptic type during the 2016 and**
886 **2017 seasons.**

887

888



889

890 **Figure 6: Boxplot of daily residual snowpack energy fluxes (a) and bar chart of total summed energy flux (b) by synoptic**
891 **type for the 2016 and 2017 seasons.**

892
893
894

Instrument	Manufacturer	Variables Measured	Accuracy
SI-111	Apogee Instruments	Surface Temperature (T_{sfc})	$\pm 0.2^{\circ}\text{C}$ - $10^{\circ}\text{C} < T < 65^{\circ}\text{C}$ \pm 0.5°C - $40^{\circ}\text{C} < T < 70^{\circ}\text{C}$
CS650	Campbell Scientific	Soil Water Content (SWC) Soil Temperature	$\pm 3\%$ SWC $\pm 5^{\circ}\text{C}$
CSAT3A	Campbell Scientific	Wind Components (u_x, u_y, u_z); Wind Speed (u) and Direction ($^{\circ}$); and Sonic Temperature	$\pm 5 \text{ cm s}^{-1}$
EC150	Campbell Scientific	H ₂ O Gas Density	2%
NOAH II	ETI Instrument Systems	Precipitation Accumulation	$\pm 0.254 \text{ mm}$
HFP01	Hukseflux	Soil Heat Flux	$< 3\%$
CNR4	Kipp and Zonen	K \downarrow , K \uparrow , L \downarrow , L \uparrow	K $< 5\%$ Daily Total L $< 10\%$ Daily Total
HMP155	Vaisala	Air Temperature (T_d) Relative Humidity (RH)	$< 0.3^{\circ}\text{C}$ $< 1.8\%$ RH
PTB110	Vaisala	Barometric Pressure	$\pm 0.15 \text{ kPa}$

895

896 **Table 1: Information on instruments used at the Pipers Creek catchment site.**

897

898

899

900

901

902

903

904

905

906

907

908
 909
 910

Synoptic Type	T1	T2	T3	T4	T5	T6	T7
Surface Characteristics	High pressure; SW winds	High pressure; WNW winds	Frontal; NW winds	High/low transition; W winds	High Pressure; NNW winds	Lee-side low; SW winds	High pressure; WNW winds
Cloud Cover (% days with any cover)	100%	75.00%	100.00%	100.00%	100.00%	100.00%	84.00%
Q_h (MJ m ⁻² day ⁻¹)	1.17	1.30	0.04	0.88	2.50	0.47	1.92
Q_e (MJ m ⁻² day ⁻¹)	-0.22	-0.64	-1.16	-0.67	-1.09	-0.51	-0.53
K_{\downarrow} (MJ m ⁻² day ⁻¹)	12.62	15.47	8.91	11.29	12.60	8.11	13.05
K_{\uparrow} (MJ m ⁻² day ⁻¹)	-9.61	-11.26	-6.97	-9.55	-9.48	-5.85	-9.60
L_{\downarrow} (MJ m ⁻² day ⁻¹)	19.53	20.16	24.95	22.08	23.59	26.57	21.38
L_{\uparrow} (MJ m ⁻² day ⁻¹)	-25.32	-26.00	-26.63	-25.74	-27.38	-26.91	-26.70
Q_g (MJ m ⁻² day ⁻¹)	0.07	0.06	0.10	0.08	0.10	0.09	0.09
Q_r (MJ m ⁻² day ⁻¹)	0.00	0.00	0.00	0.00	0.01	0.00	0.00
Q_{res} (MJ m ⁻² day ⁻¹)	-1.31	-0.43	-0.84	-0.90	1.11	0.63	-0.20
Total Number of Occurrences	15	16	44	19	22	16	31
Mean Type Duration (Days)	1.23	1.31	1.59	1.19	1.20	1.33	1.42

911

912 **Table 2: Synoptic, energy flux, and occurrence characteristics for each synoptic type. Mean Daily surface and cloud**
 913 **cover characteristics are mean values and daily energy flux values are median values.**

914

	Number of days	Energy Balance Closure		Q_{ec}	Wind Speed (ms^{-1})	
		Mean	SD		Mean	SD
T1	6	0.14	1.01	0.86	2.76	1.18
T2	7	0.83	1.33	0.17	2.65	1.43
T3	14	0.58	0.97	0.42	3.02	1.56
T4	1	-0.24	0.30	1.24	5.02	0.69
T5	9	0.71	1.08	0.29	3.48	1.37
T6	6	0.92	1.13	0.08	2.92	1.01
T7	16	0.67	1.02	0.33	2.86	1.63

915 **Table 3: Statistics on energy balance closure, error in energy balance closure (Q_{ec}) and wind speed during energy**
916 **balance closure analysis periods for each synoptic type.**